Title

Amplification of Drosophila Olfactory Responses by a DEG/ENaC Channel

Journal

Neuron, 104(5)

ISSN

0896-6273

Authors

Ng, Renny
Salem, Secilia S
Wu, Shiuan-Tze
et al.

Publication Date

2019-12-01

DOI

10.1016/j.neuron.2019.08.041

Peer reviewed

HHS Public Access

Author manuscript

Neuron. Author manuscript; available in PMC 2020 December 04.

Published in final edited form as:

Neuron. 2019 December 04; 104(5): 947–959.e5. doi:10.1016/j.neuron.2019.08.041.

Amplification of *Drosophila* olfactory responses by a DEG/ENaC channel

Renny Ng[1], **Secilia S. Salem**[1], **Shiuan-Tze Wu**[1], **Meilin Wu**[2], **Hui-Hao Lin**[1], **Andrew K. Shepherd**[1], **William J. Joiner**[2,3], **Jing W. Wang**[1], **Chih-Ying Su**[1,*]

[1]Neurobiology Section, Division of Biological Sciences, University of California San Diego, La Jolla, CA 92093, USA

[2]Department of Pharmacology, University of California San Diego, La Jolla, CA 92093, USA

[3]Center for Circadian Biology, University of California San Diego, La Jolla, CA 92093, USA

Abstract

Insect olfactory receptors operate as ligand-gated ion channels that directly transduce odor stimuli into electrical signals. However, in the absence of any known intermediate transduction steps, it remains unclear whether and how these ionotropic inputs are amplified in olfactory receptor neurons (ORNs). Here we find that amplification occurs in the *Drosophila* courtship-promoting ORNs through Pickpocket 25 (PPK25), a member of the degenerin/epithelial sodium channel family (DEG/ENaC). Pharmacological and genetic manipulations indicate that in Or47b and Ir84a ORNs, PPK25 mediates Ca^{2+}-dependent signal amplification via an intracellular calmodulin-binding motif. Additionally, hormonal signaling upregulates PPK25 expression to determine the degree of amplification, with striking effects on male courtship. Together, these findings advance our understanding of sensory neurobiology by identifying an amplification mechanism compatible with ionotropic signaling. Moreover, this study offers new insights into DEG/ENaC activation by highlighting a novel means of regulation that is likely conserved across species.

Graphical Abstract

*Lead Contact: c8su@ucsd.edu

Author contributions

R.N. performed single sensillum recordings, tip recordings, pharmacological experiments, immunostaining, bioinformatics analysis, molecular cloning and data analysis. S.S.S. performed coeloconic sensillum recordings. S-T.W. performed courtship assays. H-H.L. performed antennal lobe immunostaining. M.W. and W.J.J. performed CaM binding assays and Western blots, A.K.S. conducted qRT-PCR. R.N. J.W.W. and C-Y.S. wrote the manuscript with inputs from all authors.

Competing interests

The authors declare no competing interests.

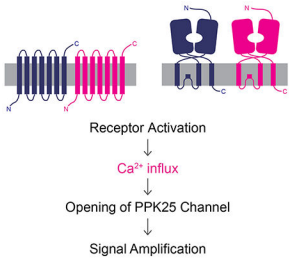

eTOC Blurb

In primary sensory neurons, little was known about whether and how ionotropic inputs are amplified. Focusing on *Drosophila* courtship-promoting olfactory neurons, Ng et al. identify an amplification mechanism downstream of Or47b and Ir84a receptor channels. Upon odor stimulation, receptor-mediated calcium influx serves as a second messenger that activates Pickpocket 25 (PPK25), DEG/ENaC whose expression is upregulated by a reproductive hormone to modulate the gain of neuronal output.

INTRODUCTION

Vertebrates detect odorants with G protein-coupled receptors (GPCRs), the activation of which triggers subsequent metabotropic signaling cascades in the olfactory receptor neurons (ORNs) to transduce chemical stimuli into electrical signals (Kaupp, 2010; Reisert and Zhao, 2011). These series of transduction events also provide opportunities to amplify input signals (Kaupp, 2010; Reisert and Zhao, 2011). In contrast, insect olfaction is initiated by ligand-gated receptor channels that lack canonical G protein interacting domains (Abuin et al., 2011; Butterwick et al., 2018; Nakagawa and Vosshall, 2009; Sato et al., 2008; Wicher et al., 2008). Although various G proteins and effectors have been implicated in the function of insect ORNs (Nakagawa and Vosshall, 2009; Wicher, 2015), it remains an open question whether those molecules play a specific role in olfactory transduction, or a regulatory role in neuronal development, maintenance and neuromodulation. Given that ligand-gated receptor channels can directly convert sensory stimuli to neuronal depolarization (Julius and Nathans, 2012), it is unclear whether and how ionotropic inputs can be amplified in the absence of any known intermediate transduction steps.

In earlier work, we found that the responses of Or47b ORNs, which detect aphrodisiac fly odors in *D. melanogaster*, increase with age in male flies (Lin et al., 2016), pointing to the possibility of signal amplification downstream of insect olfactory receptors. This age-dependent plasticity therefore presents an opportunity to investigate the mechanisms by which ionotropic sensory inputs can be amplified. Intriguingly, Or47b ORNs express a degenerin/epithelial sodium channel (DEG/ENaC) subunit named Pickpocket 25 (PPK25) (Starostina et al., 2012). Within invertebrate genomes, DEG/ENaCs constitute one of the largest ion channel families (Ben-Shahar, 2011). In mechanosensory and gustatory neurons, PPK subunits are involved in touch, proprioception, nociception, salt taste, water sensation, and recognition of contact pheromones (Adams et al., 1998; Ainsley et al., 2003; Cameron et al., 2010; Chen et al., 2010; Guo et al., 2014; Lin et al., 2005; Liu et al., 2003a, 2012; Lu et al., 2012; Starostina et al., 2012; Thistle et al., 2012; Toda et al., 2012; Vijayan et al.,

2014; Zhong et al., 2010). However, the functional role of PPK25 in olfaction remains unknown.

If PPK25 amplifies olfactory signals, how then is its activity regulated? Can it function as a transduction channel activated by intracellular second messengers downstream of receptor activation? Members of the DEG/ENaC superfamily, including the mammalian nonvoltage-gated sodium channels (SCNNs) and acid-sensing sodium ion channels (ASICs), are known to open in response to mechanical stimuli, extracellular ligands, or are otherwise constitutively active (Cameron et al., 2010; Eastwood and Goodman, 2012; Kellenberger and Schild, 2002; Younger et al., 2013). In cultured cell lines, various intracellular signaling mechanisms can influence DEG/ENaC currents by regulating channel transcription, endocytosis, degradation or translocation (Alli et al., 2015; Malik et al., 2001; Shi et al., 2002; Tokuda et al., 2002; Yu et al., 2013; Zentner et al., 1998). Post-translational modification is also known to modulate DEG/ENaC function; for example, constitutive channel activity can be regulated by CaMKII-mediated phosphorylation (Sun et al., 2013) or by protease-mediated cleavage of the extracellular domain (Rossier et al., 1997). However, the possibility of DEG/ENaC activation by direct interaction with an intracellular ligand has not been explored.

In this study, we show that signal amplification can occur downstream of ligand-gated receptor channels. We find that the age-dependent response plasticity of Or47b ORNs arises through PPK25-mediated amplification. Additionally, this mechanism is employed in another type of courtship-promoting ORN expressing the Ir84a receptor. Interestingly, the degree of amplification is determined by PPK25 expression levels, which are in turn upregulated by a reproductive hormone. Thus, a common hormone regulates these two parallel olfactory pathways to coordinate courtship behavior. Mechanistically, PPK25 operates as a transduction channel: its activation requires odor-induced Ca^{2+} influx and a calmodulin binding motif (CBM) in the N-terminal intracellular domain. This result therefore highlights a novel mechanism whereby DEG/ENaCs can be activated by second messengers, a critical feature common to all transduction channels. Moreover, similar intracellular CBMs are predicted in multiple DEG/ENaCs across animal species, suggesting an evolutionarily conserved regulatory mechanism for channels in this superfamily.

RESULTS

A DEG/ENaC channel for olfaction

We first tested whether the age-dependent response increase in the Or47b ORNs (Figure 1A–B) is mediated by mechanisms that amplify signals downstream of the Or47b ligand-gated receptor channel. We focused on PPK25, a DEG/ENaC that is expressed in these neurons (Starostina et al., 2012) (Figure 1C), where it could function as a transduction channel to amplify inputs from the Or47b receptors. We performed single-sensillum recording from *ppk25* mutant males ($ppk25^{\Delta 5\text{-}22}$, deletion of the first three exons of *ppk25*) (Lin et al., 2005) and found that the responses of their Or47b ORNs did not increase with age (Figure 1D–E) but rather remained low, at a similar level as 2-day old control males (Figure 1F). The lack of age-dependent sensitization phenotype was also observed in another *ppk25* mutant allele ($\Delta ppk25^{LexA}$), which was generated by knocking in LexA after the start

codon of *ppk25* (Figure 1F). Importantly, deleting *ppk25* eliminated the age-dependent plasticity but did not abolish Or47b ORN responses. This result suggests that PPK25 amplifies, but not directly mediates, the responses of these neurons. In agreement with this idea, genetic rescue of *ppk25* in the Or47b ORNs restored amplification of their responses (Figure 1F). We note that *ppk25* did not appear to function in female Or47b ORNs, the responses of which did not increase with age (Figure S1A–B) or decrease with *ppk25* mutation (Figure S1C–E). Together, these experiments establish that amplification of ionotropic inputs occurs downstream of the Or47b receptor, and that age-dependent response plasticity in the Or47b ORNs results from this amplification.

In a complementary experiment, we knocked down *ppk25* with RNAi selectively in the Or47b ORNs, which markedly reduced the responses in 7-day old males (Figure 1G–H) to the level of 2-day old controls (Figure 1I). We note that in 2-day old males, *ppk25* knockdown resulted in a small but significant reduction in their responses (Figure 1I), suggesting a subtle function of PPK25 in the Or47b ORNs of young males. As a control for possible off-target effects, we expressed *ppk25* RNAi in the Or22a ORNs, which do not express *ppk25* or exhibit any age-dependent plasticity, and found no changes in their responses (Figure S2).

ppk25 in ORNs impacts courtship

Using this RNAi manipulation (*Or47b-GAL4>UAS-ppk25-RNAi*), we further tested whether *ppk25* influences olfactory behavior. In a courtship competition assay, we pitted *ppk25* knockdown males against the *GAL4* and *UAS* controls and found that the knockdown males exhibited lower copulation rates than controls (Figure 2A). Among the males that copulated with females, only ~20% of them were *ppk25* knockdown flies (Figure 2B). Additionally in single-pair courtship assays, *ppk25* knockdown males exhibited prolonged courtship latency (Figure 2C), as well as a lower courtship index (Figure 2D). These results highlight the functional importance of PPK25, whereby the loss of a single channel in one subset of ORNs can profoundly compromise courtship success.

Together, our electrophysiological recordings and behavioral experiments show that *ppk25* is necessary for the amplified Or47b ORN responses in older males, and that this plasticity in the primary sensory neurons significantly influences behavior.

PPK25 levels and amplification

We next investigated the relationship between PPK25 expression levels and signal amplification. Given the age-dependent increase of Or47b ORN responses (Figure 1B), we tested whether the antennal expression of *ppk25* also increases with age. Through quantitative RT-PCR, we observed a subtle but significant increase in the *ppk25* transcript between 2- and 7-day old males (Figure 3A) but not in females (not shown). We note that *ppk25* was already expressed in the antennae of 2-day old males, consistent with the observation that *ppk25* knockdown further reduced the Or47b ORN responses of young males (Figure 1I). Interestingly, exposing newly eclosed males for two days to a juvenile hormone analog, methoprene (Jindra et al., 2013), significantly increased their *ppk25* expression (Figure 3A). In earlier work, we found that age modulates Or47b ORN responses

via juvenile hormone (Lin et al., 2016), a pleiotropic reproductive hormone that regulates male fertility and courtship behavior (Flatt et al., 2005). Specifically, methoprene treatment markedly increased the Or47b ORN responses in 2-day old males (Lin et al., 2016). Thus, the quantitative RT-PCR result suggests that age likely upregulates *ppk25* expression by means of juvenile hormone signaling. In support of this hypothesis, methoprene treatment of *ppk25* mutant males did not increase their Or47b ORN responses (Figure S3), suggesting that *ppk25* upregulation is downstream of juvenile hormone signaling. Based on these results, we predicted that increasing *ppk25* expression in the Or47b ORNs would heighten their olfactory responses.

To test this hypothesis, we used the GAL4-UAS system to increase *ppk25* expression in the Or47b ORNs, and found that this overexpression markedly increased the Or47b ORN responses in 2-day old males (Figure 3B–D). In addition, Or47b ORN responses could be further increased in 7-day old males overexpressing *ppk25* (not shown), indicating that *ppk25* levels determine the degrees of amplification. Furthermore, *Δppk25/+* heterozygous males exhibited an intermediate phenotype: their Or47b ORN responses were significantly lower than the wildtype controls but higher than the *Δppk25* homozygous mutants (Figure 3E). This haploinsufficient phenotype (Roote and Russell, 2012) further supports the notion that the level of*ppk25* expression is the key determinant of Or47b ORN response amplification. Taken together, by regulating PPK25 expression levels, juvenile hormone modulates Or47b ORN responses through flexible degrees of amplification.

To determine whether PPK25 alone can amplify the responses of ORNs which do not show age-dependent plasticity, we overexpressed *ppk25* in female Or47b ORNs (Figure S4A–B) and Or22a ORNs (Figure S4C–D) and found no response increase. These results suggest that PPK25 function requires additional components, likely other PPK subunits, which are selectively expressed in the male Or47b ORNs. Consistent with this notion, heterologous expression of PPK25 alone in HEK293 cells failed to yield any stable, detectable protein in the absence of protease inhibitors (not shown).

Having established that PPK25 expression determines the degree of amplification in Or47b ORNs, we next examined the role of Or47b receptor level in this amplification. Given that Or47b receptors are ligand-gated ion channels, elevating their expression levels could in principle also contribute to the age-dependent response increase in the Or47b ORNs. To test this possibility, we first examined male Or47b mRNA expression levels, and found that they did not change with age or methoprene treatment (Figure S5A). Furthermore, overexpression of the receptor in the Or47b ORNs along with the obligatory co-receptor, Orco (Larsson et al., 2004), did not increase their responses (Figure S5B–C), although the exogenous Or47b receptor was detected the sensory cilia where olfactory transduction occurs (Figure S5D). This result suggests that endogenous Or47b expression is already near saturation, making receptor upregulation an unlikely mechanism for age-dependent plasticity. It also argues against the possibility that PPK25 functions to regulate Or47b expression in a receptor-specific manner.

In all, our data show that Or47b ORN responses are heightened in older males as a result of elevated expression of a DEG/ENaC channel, PPK25, and not as a result of increased Or47b

receptor level. This finding establishes that transduction-mediated amplification underlies the plasticity in Or47b ORN responses.

Ca^{2+}-mediated signal amplification

What is the mechanism by which PPK25 amplifies Or47b ORN responses? All DEG/ENaC channels have two transmembrane helixes, a long extracellular loop and two short intracellular domains (Kellenberger and Schild, 2002; Zelle et al., 2013). In the N-terminal intracellular domain of PPK25, we identified a putative calmodulin (CaM) binding motif (CBM) (Rhoads and Friedberg, 1997) (Figure 4A). The CBM is highly conserved among PPK25 orthologs in multiple *Drosophila* species (Figure 4B), suggesting that this motif is critical for PPK25 function. Additionally, insect ORs are ligand-gated cation channels permeable to calcium (Butterwick et al., 2018; Sato et al., 2008; Smart et al., 2008; Wicher et al., 2008), which led us to hypothesize that receptor-mediated Ca^{2+} influx serves as a second messenger that, together with CaM, activates PPK25 by binding to its N-terminal CBM.

To test this possibility, we first employed a pharmacological approach by introducing a Ca^{2+} chelator, EGTA, in the sensillum to reduce Ca^{2+} in the extracellular lymph. We limited the duration of EGTA application to 5 min to study the acute effect of this manipulation. From single-sensillum recordings, we measured local field potential (LFP) responses as well as corresponding spike responses. The LFP response originates in the sensory cilia and thus directly reflects transduction events (Guillet and Bernard, 1972; Nagel and Wilson, 2011). We note that in the antennal trichoid sensillum of type 4 (at4), palmitoleic acid selectively activates the Or47b ORN but not the neighboring Or88a or Or65a ORNs (Lin et al., 2016) and is therefore an ideal odorant for studying the LFP responses of Or47b ORNs.

As expected, EGTA attenuated odor-evoked LFP in the Or47b ORNs of 7-day old wildtype males (Figure 4C, upper left panel), and this reduction resulted in a lower spike response (Figure 4C, lower left panel). Compared to wildtype controls, EGTA did not reduce the Or47b responses of *ppk25* mutants (Figure 4C, right panels) or those of females (Figure S6A, left panels). Additionally, EGTA did not reduce the responses of Or22a ORNs that do not express PPK25 (Figure S6B, left panels), suggesting that the attenuation was PPK25-dependent. We noticed that in *ppk25* mutants, Or47b LFP responses were slightly increased by EGTA (Figure 4C, upper right panel), likely due to its effect on Ca^{2+}-mediated adaptation (Cao et al., 2016) or on possible Ca^{2+}-mediated feedback regulation of Or47b-Orco channel conductance. Together, these results show that Ca^{2+} influx from the sensillum lymph is required for PPK25-mediated amplification in the Or47b ORNs, indicating that Ca^{2+} functions as a second messenger for signal amplification in these neurons.

To investigate the role of CaM in PPK25 function, we blocked CaM in the sensory cilia with W-7 (Hidaka et al., 1981), a membrane-permeable antagonist, and found that 5-min application of the drug also attenuated odor-evoked LFP responses in the Or47b ORNs of control males (Figure 4D). As with EGTA, this attenuation was not observed in *ppk25* mutants (Figure 4D), female Or47b ORNs (Figure S6A, right panels) or in Or22a ORNs (Figure S6B, right panels). These results indicate that functional PPK25 is required for the inhibitory effect of W-7. In addition, genetic rescue of *ppk25* in Or47b ORNs restored their

sensitivity to W-7 (Figure 4D). The simplest interpretation is that W-7 blocks CaM in the sensory cilia, which prevents PPK25 from being activated by odor-induced Ca^{2+} influx, thereby abolishing signal amplification in the Or47b ORNs.

Furthermore, to directly test whether PPK25 functions as a subunit of a DEG/ENaC channel, we applied benzamil hydrochloride, an effective DEG/ENaC antagonist for *Drosophila* PPK channels (Liu et al., 2003b; Younger et al., 2013). We found that benzamil hydrochloride significantly attenuated Or47b ORN responses in 7d wildtype males but not *ppk25* mutants (Figures S7A–B), indicating that the DEG/ENaC blocker reduces response amplification in Or47b ORNs, and that its inhibitory effect depends on PPK25. Furthermore, this supports our model in which a PPK25-containing DEG/ENaC channel functions downstream of Or47b receptor to amplify olfactory input.

Next, we addressed whether the putative CBM of PPK25 interacts with CaM. We synthesized a PPK25 CBM peptide and its mutant counterpart in which the signature 1-8-14 hydrophobic residues were replaced with glutamate (L29E, W36E & W42E, Figure 4E), a common strategy to abolish CBM function (Vocke et al., 2013). *In vitro* binding assay showed that CaM was pulled down by the wildtype CBM peptide, but not by the mutant (Figure 4E). These results indicate that the PPK25 CBM can indeed interact with CaM in a manner that depends on the signature 1-8-14 residues.

We then asked whether the CBM is required for PPK25 function *in vivo*. To address this question, we expressed either wildtype or CBM-mutated PPK25 in the Or47b ORNs of *ppk25* mutants. In the positive control, expressing wildtype *ppk25* conferred an amplified response which could then be attenuated by W-7 (Figure 4F). In contrast, CBM-mutated PPK25 yielded a smaller LFP response which was insensitive to W-7 inhibition (Figure 4G). These results suggest a critical role for the CBM in the normal function of PPK25. Of note, the LFP kinetics of the CBM mutant had a faster onset and a pronounced off response (Figure 4G), suggesting that these CBM mutations may have introduced gain-of-function abnormalities by altering the response kinetics.

Taken together, results from our pharmacological, biochemical and genetic experiments suggest that PPK25 functions as Ca^{2+}-activated transduction channel, which amplifies ionotropic input responses in the sensory cilia of Or47b ORNs. If this model were correct, PPK25 is expected to amplify ionotropic input from other Ca^{2+}-permeable receptor channels, such as channelrhodopsin-2 (ChR2) (Nagel et al., 2003). To test this hypothesis, we expressed ChR2 in Or47b ORNs and used W-7 to block any potential PPK25-mediated amplification. As a negative control, we performed the same optogenetic/pharmacological experiment in Or22a ORNs that do not express *ppk25*. In support of our model, we found that W-7 attenuated ChR2-induced responses in Or47b neurons (Figure S7C), but not in Or22a ORNs (Figure S7D), suggesting that PPK25 is also capable of amplifying responses downstream of other Ca^{2+}-permeable receptor channels. Overall, these observations suggest that PPK25 does not increase olfactory responses by modulating ligand responsiveness of Or47b, but rather through amplification of the ionotropic input.

A common transduction channel for IR and OR

Aside from the Or47b ORNs, the *ppk25* driver labeled the other type of courtship-promoting ORNs expressing the Ir84a receptor (Starostina et al., 2012) (Figure 1C), which belongs to the ionotropic receptor (IR) family (Benton et al., 2009). In addition to having distinct evolutionary origins and topologies (Benton et al., 2009; Butterwick et al., 2018; Croset et al., 2010), ORs and IRs are generally believed to involve different mechanisms when mediating olfactory responses (Cao et al., 2016; Wicher, 2015). It is therefore unclear whether PPK25 can operate downstream of Ir84a in the same manner as with Or47b. To test this possibility, we performed single-sensillum recording to determine whether PPK25 also functions as a transduction channel in the Ir84a ORNs.

Similar to the Or47b ORNs, the responses of Ir84a ORNs to their ligand, phenylacetaldehyde (Grosjean et al., 2011; Yao et al., 2005), increased with age (Figure 5A–B), indicating that amplification also occurs in this ORN subset. This age-dependent plasticity in Ir84a olfactory response is both sexually dimorphic (Figure S8) and similarly requires *ppk25:* in*ppk25* mutants, the Ir84a ORN responses were indistinguishable between 2- and 7-day old males (Figure 5C–D). As with Or47b ORNs, Ir84a ORN responses were elevated with methoprene treatment in 2-day old wildtype but not *ppk25* mutant males (Figure 5E–H). Interestingly, and in contrast to the situation in the Or47b ORNs (Figure 1), the Ir84a ORN responses of *ppk25* mutants were markedly smaller than those in 2-day old wildtype males (Figure 5B, D), suggesting that*ppk25* expression was already substantial in the Ir84a ORNs of young males.

Despite this possibility, overexpression of *ppk25* in Ir84a ORNs further elevated olfactory responses in 2-day old males (Figure 5I–J, please see the following paragraph for Figure 5K–L), indicating that PPK25 levels also determine the responses of this neuronal subset. Furthermore, the LFP responses of Ir84a ORNs were likewise sensitive to inhibition by the Ca^{2+} chelator EGTA and the CaM antagonist W-7 in a PPK25-dependent manner (Figure 6A–B, left and middle panels). We note that LFP responses to the same concentration of phenylacetaldehyde were nearly abolished in *Ir84a* mutant males (0.58 ± 0.15 mV, n=10, traces not shown). Taken together, these results indicate that PPK25 functions as a Ca^{2+}-gated transduction channel in the Ir84a ORNs to mediate signal amplification, mirroring its role in the Or47b ORNs.

Lastly we investigated whether the receptor is a key source of the Ca^{2+} that activates PPK25 in the Ir84a ORNs. The Ir84a receptor complex is permeable to Ca^{2+} and, importantly, this permeability depends on a glutamate residue in the pore domain of the receptor (Q401) (Abuin et al., 2011). Using CRISPR/Cas9-mediated genome editing (Kondo and Ueda, 2013), we engineered flies bearing the $Ir84a^{Q401R}$ mutation, which has been shown to abolish Ca^{2+} permeability (Abuin et al., 2011). Similar to the situation in *ppk25* mutants, the LFP responses of $Ir84a^{Q401R}$ mutants were reduced compared to wildtype responses, and were insensitive to EGTA or W-7 (Figure 6A–B, right panels), suggesting that Ir84a-mediated Ca^{2+} influx is the key link between PPK25 activation and the age-dependent response increase in those neurons. In support of this notion, the Ir84a ORN responses were indistinguishable between 2- and 7-day old males carrying the $Ir84a^{Q401R}$ mutation (Figure 5K–L).

Age-dependent plasticity in tarsal *ppk25*$^{+}$ GRNs.

In addition to Or47b and Ir84a ORNs, PPK25 is expressed in gustatory receptor neurons (GRNs) in the forelegs for the detection of female contact pheromones that promote male courtship (Lin et al., 2005; Liu et al., 2012, 2018; Lu et al., 2012; Starostina et al., 2012; Thistle et al., 2012; Toda et al., 2012; Vijayan et al., 2014). However, it is uncertain whether gustatory PPK25 is a pheromone receptor as suggested (Liu et al., 2018), or a transduction channel as described for olfaction. Given that all three types of *ppk25*$^{+}$ sensory neurons promote courtship, we hypothesize that the responses of tarsal *ppk25*$^{+}$ GRNs also increase with age, such that sensitivity to these aphrodisiac cues is coordinated with male fertility (Lin et al., 2016) regardless of sensory modality.

To test this hypothesis, we performed tip recording from Tm4c tarsal sensillum (Figure 7A), which houses a *ppk25*$^{+}$ GRN (Toda et al., 2012). As a negative control, we recorded from the adjacent Tm4b sensillum and observed no pheromone responses (Figure 7B). In support of our hypothesis, we found that the responses of *ppk25*$^{+}$ GRNs to their ligand, 7, 11-heptacosadiene (7,11-HD) (Pikielny, 2012; Thistle et al., 2012; Toda et al., 2012) increased with age in males (Figure 7C, left). This age-dependent plasticity was abolished in *ppk25* mutants (Figure 7C, middle) and mutants expressing PPK25 without a functional CaM-binding motif (Figure 7C, right). In comparison, the response from the neighboring *ppk25*$^{-}$ GRN to the male contact pheromone, 7-tricosene (7-T), was not affected by age or *ppk25* mutation (Figure 7D). We note that *ppk25* mutants still responded to 7,11-HD, albeit at a lower level. This result argues that as in Or47b and Ir84a ORNs, PPK25 also functions as an amplification channel in this subset of GRNs.

DISCUSSION

Here we demonstrate that ionotropic sensory inputs can be amplified in select *Drosophila* ORNs whose receptors are ligand-gated cation channels (Abuin et al., 2011; Butterwick et al., 2018; Nakagawa and Vosshall, 2009; Sato et al., 2008; Wicher et al., 2008). Pharmacological and genetic experiments reveal a simple and elegant mechanism for this amplification. Upon odor stimulation, receptor excitation allows for direct influx of Ca^{2+} which serves as a second messenger to activate a DEG/ENaC channel, PPK25, and thereby amplify ORN responses.

Ionotropic signal amplification, as described, affords remarkable versatility in sensory signaling when compared against G protein-mediated metabotropic mechanisms. In vertebrate olfaction, separate families of metabotropic receptors typically couple to different G proteins, each engaging a unique downstream signaling cascade (Kaupp, 2010). In contrast, activation of specific G proteins is not required for Ca^{2+}-mediated amplification, making it compatible with a wide variety of ionotropic receptor channels, so long as these receptors are permeable to Ca^{2+}. As evidenced in this study, PPK25 can function downstream of Or47b, Ir84a and ChR2, despite their low sequence similarity and distinct topologies (Benton et al., 2009; Butterwick et al., 2018; Nagel et al., 2003) because these receptors can flux Ca^{2+}.

Our findings highlight striking differences and commonalities between insect and vertebrate olfactory transduction. We observed surprising heterogeneity within insect olfactory transduction: PPK25 is neither expressed nor functional in another ORN type expressing Or22a, which belongs to the same receptor family as Or47b. It is unclear whether input signals in Or22a ORNs are amplified. If so, it is likely through a different mechanism. This finding indicates that insect ORNs expressing the same family of receptors do not necessarily employ the same mechanism for amplification, in contrast with vertebrate olfaction where receptors from the same family share a common signaling pathway (Kaupp, 2010). Despite this difference, the activation mechanism and function of PPK25 are remarkably similar to those of Anoctamin 2 (ANO2), a key transduction channel in vertebrate ORNs (Reisert and Zhao, 2011; Stephan et al., 2009). Specifically, both PPK25 and ANO2 are activated by calcium to amplify olfactory inputs. Although the sources of Ca^{2+} may differ—ligand-gated ion channels in insects or cyclic nucleotide-gated cation channels in vertebrates—Ca^{2+}-mediated amplification may represent a shared signaling motif between the two olfactory systems.

Interestingly, the impact of signal amplification on spike output differs between insect and vertebrate ORNs. Consistent with its role as a transduction channel, *Ano2* mutation markedly reduces odor-evoked currents (Billig et al., 2011). However, the spike output of *Ano2* knockout ORNs is higher than that of wildtype neurons (Pietra et al., 2016; Zak et al., 2018). Vertebrate ORN spike number peaks when the transduction current is largely carried by ANO2 at intermediate odor concentrations (Reisert and Matthews, 1999), suggesting a strong depolarization block whereby amplification provides negative feedback to clamp total spike output (Zak et al., 2018). In contrast, the LFP and spike responses of insect ORNs both peak at saturating odor concentrations (Zhang et al., 2019). As such, blocking PPK25-mediated amplification not only reduces LFP response, but also total spike number (Figures 4 and 6). Therefore, signal amplification in insect ORNs may predominantly serve to modulate the gain of neuronal output.

What is the functional significance of PPK25 in the Or47b and Ir84a ORNs? Notably, these are the only ORN types known to promote courtship in *D. melanogaster* males, whose fertility and courtship drive increase and peak at about 7 days of age (Dweck et al., 2015; Grosjean et al., 2011; Lin et al., 2016; Long et al., 1980). Male mating drive is highly influenced by external olfactory cues, including the availability of mates and food signaled by Or47b and Ir84a ORNs, respectively (Grosjean et al., 2011; Lin et al., 2016). Remarkably, the responses of both ORN types exhibit age-dependent plasticity (Figures 1, 5), which is coordinated by the same reproductive hormone—juvenile hormone—through upregulation of PPK25 expression in older males (Lin et al., 2016) (Figures 3, 5 and S3). The expression level of PPK25 in turn determines the ORN response magnitude, with striking impacts on courtship (Figure 2). Therefore, flexibility over this biologically salient behavior is afforded by the dynamic regulation of PPK25 expression, which heightens males' sensitivity to food and mate odors at their age of peak fertility. This upregulation of PPK25 provides a molecular mechanism for how sex-specific refinements of olfactory circuits are achieved via hormonal signaling (Knoedler and Shah, 2018).

The critical role of the intracellular CBM in PPK25 function (Figures 4E, G) argues that Ca^{2+}/CaM activates the channel by directly interacting with this motif. Such regulation contrasts sharply with previously reported mechanisms, in which Ca^{2+}/CaM indirectly modulates ENaC activity through intermediate proteins. For example in cultured *Xenopus* cells, Ca^{2+}/CaM can inhibit ENaC currents by interacting with MARCKS (myristoylated alanine-rich C kinase substrate) to modulate channel open probability, and also by activating CaMKII to regulate ENaC apical trafficking (Alli et al., 2015). Together, these findings highlight the complexity of interactions between Ca^{2+}/CaM and neuronal DEG/ENaC.

The results described in this study further advance our understanding of DEG/ENaC channel activation. The gating mechanisms for this family of sodium channels are known to be highly diverse: some open in response to mechanical stimuli, others to extracellular ligands, and still others are constitutively active (Cameron et al., 2010; Eastwood and Goodman, 2012; Kellenberger and Schild, 2002; Younger et al., 2013). In light of our findings, it is possible that other members of the DEG/ENaC superfamily may also be directly activated by intracellular second messengers, allowing them to function as transduction channels to amplify sensory inputs. In support of this notion, similar N-terminal intracellular CBMs were bioinformatically identified in multiple members of the DEG/ENaC superfamily across species—including worm, fruit fly, mosquito, mouse and human (Table 1)—suggesting that those channels have the potential to function as Ca^{2+}-activated transduction channels.

STAR METHODS

LEAD CONTACT AND MATERIALS AVAILABILITY

Fly lines generated in this study are available upon request. Further information and requests for reagents may be directed to and will be fulfilled by the Lead Contact, Chih-Ying Su (c8su@ucsd.edu).

EXPERIMENTAL MODEL AND SUBJECT DETAILS

Drosophila melanogaster were reared on standard white cornmeal food at 25°C in an incubator with a 12-hr light/dark cycle. Experimental flies were collected at eclosion, separated by sex, raised in groups of ten and transferred to new vials with fresh food every other day. Recordings were performed on adult flies 2 or 7 days after eclosion as indicated. Table S1 lists genotypes for all experiments.

METHOD DETAILS

Single-sensillum recording—To prepare an antenna for recording, a fly was wedged into the narrow end of a truncated 200-μl pipette tip to expose the antenna, which was subsequently stabilized between a tapered glass microcapillary tube and a coverslip covered with double-sided tape. Extracellular single-sensillum recordings were performed essentially as described (Ng et al., 2017). Briefly, adult hemolymph-like (AHL) solution was used to fill a glass reference electrode, which was inserted into either the eye (for Or22a or Ir84a ORN recordings) or the clypeus (for Or47b ORN recordings). An AHL-filled recording electrode was then inserted into the sensillum of interest. For trichoid and coeloconic recordings, no more than two sensilla were recorded per fly. For ab3 recordings, two or three different

sensilla were recorded from each fly. AC signals (100-20k Hz) and DC signals were simultaneously recorded on an NPI EXT-02F amplifier (ALA Scientific Instruments) and digitized at 5 kHz with Digidata 1550 (Molecular Devices). ORN spikes were sorted and analyzed offline using Clampfit 10 (Molecular Devices) and Igor Pro (WaveMetrics). Spike responses were averaged, binned at 50 ms, and smoothed using a binomial algorithm to obtain peri-stimulus time histograms (PSTHs). For dosage curves and statistical analysis, responses were quantified by subtracting the pre-stimulus spike rate (1 s) from the peak spike response during odorant stimulation (adjusted peak responses).

The at4 sensillum, which houses the Or47b ORNs, was identified based on the location of the sensillum on the antenna and the number of compartmentalized neurons, as described (Ng et al., 2017). The identity of the sensillum (ac4) housing the Ir84a ORNs (ac4A) was determined based on sensillum morphology, location (distal region of the antenna) and the responsiveness of the neighboring neurons to phenylethylamine (Grosjean et al., 2011).

Odor stimuli—In this study, short odor pulses were used in order to minimize the possible impact of adaptation (Cao et al., 2016). One hundred microliters of each paraffin oil-diluted odorant was added to a filter disc inserted into a glass Pasteur pipette. Odor stimuli were delivered to the antenna via 500-ms (ethyl hexanoate, Sigma 148962) or 250-ms (phenylacetaldehyde, Sigma W287407) air pulses at 200 ml/min into the main airstream (2000 ml/min). A shorter pulse of phenylacetaldehyde was used in order to prevent prolonged responses in the Ir84a ORNs so as to facilitate the dose-response experiments. Palmitoleic acid (Cayman 9001798) was diluted in ethanol, applied as a 4.5-μl portion to a filter disc and delivered via a 500-ms air pulse at 250 ml/min directly to the antenna from close range as described (Ng et al., 2017).

Optogenetic stimulation—Newly eclosed male flies expressing the H134R-ChR2 transgene (Pulver et al., 2009) in target ORNs were reared in constant darkness for 7 days on fly food supplemented with 100 μM all *trans*-retinal (Sigma). Flies were transferred to fresh retinal food one day prior to experiments. A light stimulus was generated via a blue LED (470 nm, Universal LED Illumination System, pE-4000, Cool LED). Light pulses (500-ms duration, 20% output) were controlled by Clampex 10.4 (Molecular Devices).

Tip recording of tarsal taste sensilla—Electrophysiological recordings were performed with 2d and 7d male flies that were collected at eclosion, separated by sex, and raised in groups of ten. Flies were decapitated 1-2 hr prior to experiments. To prepare the legs for recording, a decapitated fly was first pinned down on a Sylgard plate, the surface of which was covered with a piece of double-sided tape (Ling et al., 2014). The thorax and tibias of the fly were further stabilized with human hairs to minimize movements. A reference electrode containing 1 mM KCl was inserted into the thorax. For stimulation, contact was made between the sensillum tip and the recording electrode (10-15 μm tip diameter) filled with the tested compound (Toda et al., 2012). The final pheromone concentrations were 20 ng/μl for 7,11-heptacosadiene (Cayman 10012567, 10 μg/μl in ethanol) and 10 ng/μl for 7-tricosene (Cayman 9000313, 10 μg/μl in hexane) diluted in 1 mM KCl. AC signals (100-20k Hz) were recorded on an NPI EXT-02F amplifier (ALA Scientific Instruments) and digitized at 5 kHz with Digidata 1550 (Molecular Devices).

From each foreleg, only one pair of Tm4c and Tm4b sensilla was recorded. Both forelegs were examined for each fly. Spike activity was analyzed offline using Clampfit 10 (Molecular Devices), and the average responses were calculated as the total number of spikes fired above noise level for 1 s after contact.

Courtship assays—Flies were raised on standard cornmeal food containing molasses at 25°C in an incubator with a 12-hr light/dark cycle. *UAS-ppk25-RNAi* and *Or47b-GAL4* were backcrossed to wildtype Berlin (w^-) for eight generations. Flies were collected at eclosion, separated by sex, raised in groups of ten and transferred to new vials with fresh food every other day.

The courtship competition assay was modified from a previous study (Lin et al., 2016). Briefly, three 7-day old naive males of different genotypes and one 3-day old virgin female (*Canton-S*) were loaded in a mating chamber (4 cm in diameter and 1 cm in height, volume: 12.56 cm^3) positioned on top of a Petri dish containing diluted fly food (60% in water). The base of the chamber is made of a piece of gauze to allow flies access to food odors. To facilitate fly identification, two males of different genotypes were dusted with fluorescent dyes (UVXPBB and UVXPBR, Llewellyn Data Processing LLC) ~20 hr prior to experiments. Dye application was alternated among genotypes across experiments to minimize dye-induced behavioral bias. Courtship competition assays were conducted at 25°C, 50% relative humidity under 660-nm red light. For each experiment, 30 matches were set up and only trials in which copulation occurred within 2 hr were included in the analysis. Copulation was visually confirmed, and then a UV flashlight was turned on briefly to visualize the fluorescent dye in order to identify the mated males. The genotype of the copulated males and the time of copulation were recorded during the 2-hr period. The data were analyzed in MATLAB (MathWorks).

For single-pair courtship assay, one 7-day old naive male and one 3-day old virgin female (*Canton-S*) were loaded into each chamber (1 cm in diameter and 0.5 cm in height, volume: 0.4 cm^3) of a mating wheel (Siegel and Hall, 1979) with 850-nm back illumination. Single-pair courtship assays were conducted under white light at 25°C, 50% relative humidity. Courtship behavior was recorded at 15 frames/s with a digital camera (Flea3, Point Grey), the lens of which was fitted with an IR-pass filter. Scoring was performed offline by a blinded observer. Courtship latency was defined as the time required for the male to initiate courtship. Courtship index was defined as the percentage of time during the first 10 min of the assay in which the male fly engaged in courtship activity (chasing, orientation, wing extension, attempted copulation and copulation).

Quantitative RT-PCR—Wildtype Berlin flies were collected within 24 hr post-eclosion, segregated by sex, and aged to either 2 days or 7 days. Three different conditions were examined: 2d males, 7d males, 2d males treated with methoprene for two days (see “Pharmacology” section below). Anesthetized flies were dipped in liquid nitrogen and antennae were brushed off using a needle into a 1.5 ml centrifuge tube filled with liquid nitrogen. For each condition, antennae were collected from 12 sample sets of 50 flies each and stored at −80°C. RNA was extracted from each antennal sample using the QIAGEN RNeasy Mini and QIAshredder kits. A hand-held pestle drill was used during extraction.

Antennal cDNA was prepared from the mRNA using Invitrogen Superscript VILO MasterMix. Quantitative PCR (qPCR) was performed on the Bio-Rad CFX machine. PrimeTime® qPCR assays from Integrated DNA Technologies used the following primers and probes:

ppk25: Forward primer – GTTAAAATCCCGCCAGAACTG

Probe - 5HEX/TCCTGTGTT/ZEN/TCTAGTTTGCCGTAGGG/3IABkFQ

Reverse primer - CAATTACTCAAATAGCCGCACTG

Or47b: Forward primer: TCAAATCTCAGCCTTCTGCG

Probe: 5HEX/CAGCAAACT/ZEN/CAGAAAGGCGCGAAC/3IABkFQ

Reverse primer: CTTCTTGTTGGGATACTGGC

rp49: Forward primer - TCGATATGCTAAGCTGTCGC

Probe - 5HEX/ATCAGATAC/ZEN/TGTCCCTTGAAGCGGC/3IABkFQ

Reverse primer - TTCTTGAATCCGGTGGGC

rp49 served as a reference gene to which *ppk25* and *Or47b* were normalized. RT-qPCR was performed with each PrimeTime® assay in three technical replicates for each cDNA sample using Bio-Rad iTaq Universal Probes Mastermix (final primer concentration: 500 nM; final probe concentration: 250 nM). CT values were recorded with Bio-Rad CFX Manager software. Statistical analysis was performed based on the CT values. For each set of technical replicates, an outlier was discarded and the average of the two remaining replicates was used as the representative value for the set to determine relative transcript levels.

Bioinformatics—The calmodulin binding motifs (CBM) in PPK25 and other DEG/ENaC members were predicted and scored using the Calmodulin Target Database (http://calcium.uhnres.utoronto.ca/ctdb/no_flash.htm). The most likely binding site is identified as a series of residues with scores of 9s. Transmembrane domains were predicted using TMHMM Server v. 2.0 (http://www.cbs.dtu.dk/services/TMHMM/). The 1-8-14 motif of PPK25 CBM was determined using the Calmodulation database and Meta-analysis predictor (http://cam.umassmed.edu).

The full-length amino acid sequence of *D. melanogaster* PPK25 (NP_995766 or CG33349) was used as a query to BLAST search orthologs of PPK25 in other *Drosophila* species (E value = 0, *D. simulans*, XP_016026221; *D. sechellia*, XP_002032669; *D. yakuba*, XP_002089400; *D. erecta*, XP_001970701; *D. ananassae*, XP_001960001; *D. persimilis*, XP_002015545; *D. willistoni*, XP_002063147; *D. busckii* , ALC41546; *D. bipectinata*, XP_017093595; *D. suzukii*, XP_016940277; *D. kikkawai*, XP_017031054; *D. eugracilis*, XP_017078184; *D. elegans*, XP_017125733; *D. ficusphila*, XP_017050268; *D. biarmipes*, XP_016957828; *D. rhopaloa*, XP_016978723). Similarly, the full-length amino acid sequence of *D. melanogaster* PPK23 (NP_573220.2 or CG8527) was used as a query to

BLAST search orthologs of PPK23 in other *Drosophila* species (E value = 0, *D. simulans*, XP_016039787.1; *D. sechellia*, XP_002042389.1; *D. yakuba*, XP_002101509.2; *D. erecta*, XP_001977571.2; *D. ananassae*, XP_001965652.2; *D. willistoni*, XP_002064047.2; *D. busckii* , ALC49816.1; *D. bipectinata*, XP_017094379.1; *D. suzukii*, XP_016938912.1; *D. kikkawai*, XP_017034621.1; *D. eugracilis*, XP_017067301.1; *D. elegans*, XP_017112672.1; *D. ficusphila*, XP_017055937.1; *D. biarmipes*, XP_016948023.1; *D. rhopaloa*, XP_016979919.1). Multiple sequence alignments of the calmodulin binding motifs from different *Drosophila* species were performed with Clustal Omega (EMBL-EBI).

DNA constructs and *Drosophila* transgenesis—The coding region of *ppk25* was amplified from antennal cDNA (wildtype Berlin) and cloned into pRK5-(C)-myc to add a myc epitope (EQKLISEEDL) to the C-terminus of PPK25. The *ppk25* sequence completely matched the reference CDS in the FlyBase. The CBM 1-8-14 mutations of *ppk25* were generated by standard site-directed mutagenesis to introduce three point mutations (I29E, W36E and W42E) in the calmodulin binding motif (GENEWIZ). To facilitate Gateway Cloning (ThermoFisher Scientific), the attB1 and attB2 sites were included in the primers and then added to the ends of PCR amplicons, which were subsequently cloned into pDONR221 vectors via BP Clonase II (Life Technologies) and recombined into the pBID-UASC-G destination vector (Wang et al., 2012) using LR Clonases II (Life Technologies) for transgenic injections. All DNA constructs were verified by sequencing. *Drosophila* transgenic lines were derived from germline transformations using the ΦC31 integration systems (Markstein et al., 2008). *UAS-ppk25-myc* and *UAS-ppk25 (CBM 1-8-14)-myc* were inserted into the 9725 landing site on the third chromosome (BestGene).

$\Delta ppk25^{LexA}$ and $Ir84a^{Q401R}$ receptor mutant flies were generated by Wellgenetics Inc. using CRISPR/Cas9-mediated genome editing (Kondo and Ueda, 2013). $\Delta ppk25^{LexA}$ was generated by knocking in LexA downstream of the start codon of *ppk25*. A 40-bp sequence (from the 4^{th}-43^{th} nucleotide of *ppk25*) was deleted and replaced by the knock-in cassette containing nls-LexA::p65-LoxP-3xP3-RFP-LoxP by homology-dependent repair. For $Ir84a^{Q401R}$, the cassette Q401R-PBacDsRed containing two PBac terminals, 3xP3-DsRed and two homology arms with the point mutation Q401R (tatctgCAAcagggc to tatctgCGTcagggc) were cloned into pUC57-Kan as the donor plasmid for homology dependent repair. The donor, gRNAs and hs-Cas9 plasmids were injected into embryos of the control strain w^{1118}. F1 flies carrying selection marker (3xP3-DsRed or 3xP3-RFP) were validated by genomic PCR and sequencing. The fluorescent selection marker was subsequently excised by the Cre recombinase for $\Delta ppk25^{LexA}$ or by PiggyBac(PBac) transposition for $Ir84a^{Q401R}$. Successful excision was determined by genomic PCR and further verified with DNA sequencing of the PCR products.

Immunohistochemistry—Seven-day old male files expressing myc-tagged Or47b in the target ORNs were anesthetized on ice, with their heads aligned in a collar, covered with Cryo-OCT (Tissue-Tek, Fisher Scientific), and frozen on dry ice as described (Saina and Benton, 2013). Antennal sections (14 μm) were collected on Superfrost Plus microscope slides (Fisher Scientific), fixed with 4% paraformaldehyde and stained with rabbit α-myc 1:250 (71D10, Cell Signaling Technology) and 21A6 monoclonal antibody 1:200 (DSHB)

before incubating with the secondary antibodies, Alexa 647 goat α-rabbit 1:200 (Life Technologies) and Alexa 568 goat α-mouse 1:250 (Life Technologies). The sections were then mounted in Fluoromount-G™ (ThermoFisher). For antennal lobe imaging, the brains from 7-day old males were fixed in 4% paraformaldehyde and stained with rabbit α-GFP 1:500 (Life Technologies) and mouse monoclonal nc82 1:50 (DHSB) before incubating with the secondary antibodies, Alexa goat α-rabbit 488 1:500 (Life Technologies) and Alexa 647 goat α-mouse 1:500 (Life Technologies). The brains were mounted in FocusClear™ (CelExplorer). Confocal images were acquired with Zeiss LSM 510 (antennal lobe) or LSM 880 (antenna section) and processed with ImageJ.

Pharmacology—All pharmacological manipulations were performed in 7d males. EGTA (Sigma) was used to chelate Ca^{2+} in the sensillum lymph and W-7 (Santa Cruz Biotechnology), a membrane permeable calmodulin antagonist, was used to block calmodulin in the sensory cilia. Benzamil hydrochloride hydrate (Sigma) is an amiloride derivative that blocks DEG/ENaC channels. EGTA (5 mM in AHL, pH ~7), W-7 solution (500 μM in AHL) and benzamil hydrochloride (400 μM in AHL) were prepared daily prior to experiments and delivered inside the sensillum via the recording glass electrode through diffusion. High concentrations of drugs were used to compensate for possible dilution of the drugs in the sensillum lymph. Responses of an ORN to identical odor stimuli were recorded twice to determine the effect of drugs; the first recording was performed immediately after electrode insertion (control response) and the second recording after 5 min, during which time the electrode remained inside the sensillum to allow the compound to take effect. The application duration was empirically determined to be the shortest time required for a robust, observable effect on the olfactory responses in the wildtype Or47b or Ir84a ORNs. Although further attenuation was observed with longer application (not shown), the 5-min duration was used to minimize the possibility of affecting other cellular processes in the ORNs by the drugs. Of note, our stimulus paradigm using a single short odor pulse (0.25 or 0.5 s) does not address the possible function of CaM in ORN sensitization (Mukunda et al., 2016) or other aspects of Ca^{2+}-regulated ORN physiology (Cao et al., 2016; Wicher, 2015).

Methoprene treatment—Methoprene (0.25%, v/v in ethanol, Sigma 33375) was prepared daily prior to application. Ten microliters of methoprene or solvent (ethanol) was applied to the surface of medium and the vials containing treated food were left in a fume hood for 30 min to allow ethanol to evaporate. Male flies were collected upon eclosion and raised in methoprene- or solvent-treated food in groups of ten. The flies were transferred to fresh vials of treated food every day. Recordings were performed on 2-day old males that have been reared on treated food for two days.

CaM binding assay—PPK25-N-CBM peptide [KGGGPYLARRDLHWAERLFWTF-NH2] and mutant peptide [KGGGPYEARRDLHEAERLFETF-NH2] (Biomatik) were solubilized in PBS and coupled to NHS-agarose (Pierce) according to the manufacturer's protocol. Human recombinant calmodulin (Enzo Life Sciences) was solubilized in Buffer A (50 mM Tris pH 7.4, 0.1% β-mercaptoethanol, 0.1% Triton X-100, and 5 mM $CaCl_2$) at 1 mg/ml. Fifty microliters of the peptide or buffer A (no-peptide control) was incubated with 4 μg of recombinant calmodulin in 500 μl of Buffer A with Complete protease inhibitors

(Roche) for 2 hours at 4°C with end-over-end rotation. Five percent of the input calmodulin was saved as the input fraction. After incubation, 5% of the supernatant was saved as the unbound fraction. The beads were washed twice with 1 ml of PBST and then resuspended in 50 μl of Buffer A+LDS sample buffer (1:1, Life Technologies). The input, unbound and immunoprecipitated fractions were denatured at 95°C and loaded on 4-12% NuPage (LIfeTechnologies) gels for electrophoresis and Western blotting with polyclonal anti-calmodulin antibody (#4830, Cell Signaling).

QUANTIFICATION AND STATISTICAL ANALYSIS

All data were analyzed using Excel or MATLAB. Coefficients and the standard deviations of the fits with Hill Equation were generated in Igor Pro 6.3. Data are presented as mean ± s.e.m. $P < 0.05$ was considered to be statistically significant and is presented as * $P < 0.05$, ** $P < 0.005$, or *** $P < 0.0005$. For data analyzed by ANOVA followed by Tukey's test, $P < 0.05$ was considered to be statistically significant and different groups are denoted by different letters. All statistical details can be found in the figure legends. Unpaired two-tailed *t*-test was performed in Figure 1B, E, F, H; Figure 3A, C; Figure 5B, D, F, H, J, L; Figure 7C, D; Figure S1B, D; Figure S2B, D; Figure S3B; Figure S4B, D; Figure S5A, C; Figure S8B. Paired two-tailed *t*-test was performed in Figure 4C, D, F, G; Figure S6A, B; Figure S7A, B, C, D. ANOVA followed by Tukey's test was performed in Figure 1I; Figure 2B, C, D; Figure 3D, E; Figure 6A, B; Figure S1E.

DATA AND CODE AVAILABILITY

This study did not generate/analyze datasets/code.

Supplementary Material

Refer to Web version on PubMed Central for supplementary material.

Acknowledgements

We thank Gareth Thomas for advice on the design of the CaM binding assay; Frederick Ling for advice on tip recording of tarsal sensilla; Vanessa Martin for help with courtship analysis; Ardem Patapoutian, Larry Squire, Samer Hattar and Johannes Reisert for comments on the manuscript, and Xiangyu Ren for generating *myc-tagged ppk25* transgenic constructs.

Funding

This work was supported by a Ray Thomas Edwards Foundation Career Development Award and NIH grants (R01DC016466 and R01DC015519) to C-Y.S., R01DC016466 and R01DC009597 to J.W.W. and R01GM125080 to W.J.J.

REFERENCES

Abuin L, Bargeton B, Ulbrich MH, Isacoff EY, Kellenberger S, and Benton R (2011). Functional architecture of olfactory ionotropic glutamate receptors. Neuron 69, 44–60. [PubMed: 21220098]

Adams CM, Anderson MG, Motto DG, Price MP, Johnson WA, and Welsh MJ (1998).Ripped Pocket and Pickpocket, novel Drosophila DEG/ENaC subunits expressed in early development and in mechanosensory neurons. J. Cell Biol 140, 143–152. [PubMed: 9425162]

Ainsley JA, Pettus JM, Bosenko D, Gerstein CE, Zinkevich N, Anderson MG, Adams CM, Welsh MJ, and Johnson WA (2003). Enhanced locomotion caused by loss of the Drosophila DEG/ENaC protein Pickpocket1. Curr. Biol 13, 1557–1563. [PubMed: 12956960]

Alli AA, Bao H-F, Liu B-C, Yu L, Aldrugh S, Montgomery DS, Ma H-P, and Eaton DC (2015). Calmodulin and CaMKII modulate ENaC activity by regulating the association of MARCKS and the cytoskeleton with the apical membrane. Am. J. Physiol. Physiol 309, F456–F463.

Ben-Shahar Y (2011). Sensory functions for Degenerin/Epithelial Sodium Channels (DEG/ENaC). Adv. Genet 76, 2–26.

Benton R, Vannice KS, Gomez-Diaz C, and Vosshall LB (2009). Variant ionotropic glutamate receptors as chemosensory receptors in Drosophila. Cell 136, 149–162. [PubMed: 19135896]

Billig GM, Pál B, Fidzinski P, and Jentsch TJ (2011). Ca^{2+}-activated Cl^- currents are dispensable for olfaction. Nat. Neurosci 14, 763–769. [PubMed: 21516098]

Butterwick JA, del Marmol J, Kim KH, Kahlson MA, Rogow JA, Walz T, and Ruta V (2018). Cryo-EM structure of the insect olfactory receptor Orco. Nature 560, 447–452. [PubMed: 30111839]

Cameron P, Hiroi M, Ngai J, and Scott K (2010). The molecular basis for water taste in Drosophila. Nature 465, 91–95. [PubMed: 20364123]

Cao L-H, Jing B-Y, Yang D, Zeng X, Shen Y, Tu Y, and Luo D-G (2016). Distinct signaling of Drosophila chemoreceptors in olfactory sensory neurons. Proc. Natl. Acad. Sci. U. S. A 113, E902–11. [PubMed: 26831094]

Chen Z, Wang Q, and Wang Z (2010). The amiloride-sensitive epithelial Na^+ channel PPK28 is essential for Drosophila gustatory water reception. J. Neurosci 30, 6247–6252. [PubMed: 20445050]

Croset V, Rytz R, Cummins SF, Budd A, Brawand D, Kaessmann H, Gibson TJ, and Benton R (2010). Ancient protostome origin of chemosensory ionotropic glutamate receptors and the evolution of insect taste and olfaction. PLoS Genet. 6, e1001064. [PubMed: 20808886]

Dweck HKM, Ebrahim SAM, Thoma M, Mohamed AAM, Keesey IW, Trona F, Lavista-Llanos S, Svatos A, Sachse S, Knaden M, et al. (2015). Pheromones mediating copulation and attraction in Drosophila. Proc. Natl. Acad. Sci 112, 2829–2835. [PubMed: 25730874]

Eastwood AL, and Goodman MB (2012). Insight into DEG/ENaC channel gating from genetics and structure. Physiology 27, 282–290. [PubMed: 23026751]

Flatt T, Tu MP, and Tatar M (2005). Hormonal pleiotropy and the juvenile hormone regulation of Drosophila development and life history. Bioessays 27, 999–1010. [PubMed: 16163709]

Grosjean Y, Rytz R, Farine J-P, Abuin L, Cortot J, Jefferis GSXE, and Benton R (2011). An olfactory receptor for food-derived odours promotes male courtship in Drosophila. Nature 478, 236–240. [PubMed: 21964331]

Guillet JC, and Bernard J (1972). Shape and amplitude of the spikes induced by natural or electrical stimulation in insect receptors. J. Insect Physiol 18, 2155–2171.

Guo Y, Wang Y, Wang Q, and Wang Z (2014). The role of PPK26 in Drosophila larval mechanical nociception. Cell Rep. 9, 1183–1190. [PubMed: 25457610]

Hallem EA, Ho MG, and Carlson JR (2004). The molecular basis of odor coding in the Drosophila antenna. Cell 117, 965–979. [PubMed: 15210116]

Hidaka H, Sasaki Y, Tanaka T, Endo T, Ohno S, Fujii Y, and Nagata T (1981). N-(6-aminohexyl)-5-chloro-1-naphthalenesulfonamide, a calmodulin antagonist, inhibits cell proliferation. Proc. Natl. Acad. Sci. U. S. A 78, 4354–4357. [PubMed: 6945588]

Jindra M, Palli SR, and Riddiford LM (2013). The juvenile hormone signaling pathway in insect development. Annu. Rev. Entomol 58, 181–204. [PubMed: 22994547]

Julius D, and Nathans J (2012). Signaling by sensory receptors. Cold Spring Harb. Perspect. Biol 4, 1–14.

Kaupp UB (2010). Olfactory signalling in vertebrates and insects: Differences and commonalities. Nat. Rev. Neurosci 11, 188–200. [PubMed: 20145624]

Kellenberger S, and Schild L (2002). Epithelial sodium channel/Degenerin family of ion channels: A variety of functions for a shared structure. Physiol. Rev 82, 735–767. [PubMed: 12087134]

Knoedler JR, and Shah NM (2018). Molecular mechanisms underlying sexual differentiation of the nervous system. Curr. Opin. Neurobiol 53, 1–17. [PubMed: 29694927]

Kondo S, and Ueda R (2013). Highly Improved gene targeting by germline-specific Cas9 expression in Drosophila. Genetics 195, 715–721. [PubMed: 24002648]

Larsson MC, Domingos AI, Jones WD, Chiappe ME, Amrein H, and Vosshall LB (2004). Or83b encodes a broadly expressed odorant receptor essential for Drosophila olfaction. Neuron 43, 703–714. [PubMed: 15339651]

Lin H, Mann KJ, Starostina E, Kinser RD, and Pikielny CW (2005). A Drosophila DEG/ENaC channel subunit is required for male response to female pheromones. Proc. Natl. Acad. Sci. U. S. A 102, 12831–12836. [PubMed: 16129837]

Lin H-H, Cao D-S, Sethi S, Zeng Z, Chin JSR, Chakraborty TS, Shepherd AK, Nguyen CA, Yew JY, Su C-Y, et al. (2016). Hormonal modulation of pheromone detection enhances male courtship success. Neuron 90, 1272–1285. [PubMed: 27263969]

Ling F, Dahanukar A, Weiss LA, Kwon JY, and Carlson JR (2014). The molecular and cellular basis of taste coding in the legs of Drosophila. J. Neurosci 34, 7148–7164. [PubMed: 24849350]

Liu L, Leonard AS, Motto DG, Feller MA, Price MP, Johnson WA, and Welsh MJ (2003a). Contribution of Drosophila DEG/ENaC genes to salt taste. Neuron 39, 133–146. [PubMed: 12848938]

Liu L, Johnson W. a, and Welsh MJ (2003b). Drosophila DEG/ENaC pickpocket genes are expressed in the tracheal system, where they may be involved in liquid clearance. Proc. Natl. Acad. Sci. U. S. A 100, 2128–2133. [PubMed: 12571352]

Liu T, Starostina E, Vijayan V, and Pikielny CW (2012). Two Drosophila DEG/ENaC channel subunits have distinct functions in gustatory neurons that activate male courtship. J. Neurosci. 32, 11879–11889. [PubMed: 22915128]

Liu T, Wang Y, Tian Y, Zhang J, Zhao J, and Guo A (2018). The receptor channel formed by ppk25, ppk29 and ppk23 can sense the Drosophila female pheromone 7,11-heptacosadiene. Genes, Brain Behav. 1–10.

Long CE, Markow TA, and Yaeger P (1980). Relative male age, fertility, and competitive mating success in Drosophila melanogaster. Behav. Genet 10, 163–170. [PubMed: 6783024]

Lu B, LaMora A, Sun Y, Welsh MJ, and Ben-Shahar Y (2012). ppk23-dependent chemosensory functions contribute to courtship behavior in Drosophila melanogaster. PLoS Genet. 8, e1002587. [PubMed: 22438833]

Malik B, Schlanger L, Al-Khalili O, Bao HF, Yue G, Price SR, Mitch WE, and Eaton DC (2001). ENaC degradation in A6 cells by the ubiquitin-proteosome proteolytic pathway. J. Biol. Chem 276, 12903–12910. [PubMed: 11278712]

Markstein M, Pitsouli C, Villalta C, Celniker SE, and Perrimon N (2008). Exploiting position effects and the gypsy retrovirus insulator to engineer precisely expressed transgenes. Nat. Genet 40, 476–483. [PubMed: 18311141]

Mukunda L, Miazzi F, Sargsyan V, Hansson BS, and Wicher D (2016). Calmodulin affects sensitization of Drosophila melanogaster odorant receptors. Front. Cell. Neurosci 10, 1–11. [PubMed: 26858601]

Nagel KI, and Wilson RI (2011). Biophysical mechanisms underlying olfactory receptor neuron dynamics. Nat. Neurosci 14, 208–216. [PubMed: 21217763]

Nagel G, Szellas T, Huhn W, Kateriya S, Adeishvili N, Berthold P, Ollig D, Hegemann P, and Bamberg E (2003). Channelrhodopsin-2, a directly light-gated cation-selective membrane channel. Proc. Natl. Acad. Sci. U. S. A 100, 13940–13945. [PubMed: 14615590]

Nakagawa T, and Vosshall LB (2009). Controversy and consensus: noncanonical signaling mechanisms in the insect olfactory system. Curr. Opin. Neurobiol 19, 284–292. [PubMed: 19660933]

Ng R, Lin H-H, Wang JW, and Su C-Y (2017). Electrophysiological recording from Drosophila trichoid sensilla in response to odorants of low volatility. J. Vis. Exp e56147.

Pietra G, Dibattista M, Menini A, Reisert J, and Boccaccio A (2016). The Ca^{2+}-activated Cl^{-} channel TMEM16B regulates action potential firing and axonal targeting in olfactory sensory neurons . J. Gen. Physiol 148, 293–311. [PubMed: 27619419]

Pikielny CW (2012). Sexy DEG/ENaC channels involved in gustatory detection of fruit fly pheromones. Sci. Signal 5, pe48. [PubMed: 23131844]

Pulver SR, Pashkovski SL, Hornstein NJ, Garrity P. a, and Griffith LC (2009). Temporal dynamics of neuronal activation by Channelrhodopsin-2 and TRPA1 determine behavioral output in Drosophila larvae. J. Neurophysiol 101, 3075–3088. [PubMed: 19339465]

Reisert J, and Matthews HR (1999). Adaptation of the odour-induced response in frog olfactory receptor cells. J. Physiol 519, 801–813. [PubMed: 10457092]

Reisert J, and Zhao H (2011). Response kinetics of olfactory receptor neurons and the implications in olfactory coding. J. Gen. Physiol 138, 303–310. [PubMed: 21875979]

Rhoads AR, and Friedberg F (1997). Sequence motifs for calmodulin recognition. FASEB J. 11, 331–340. [PubMed: 9141499]

Roote J, and Russell S (2012). Toward a complete Drosophila deficiency kit. Genome Biol. 13, 6–8.

Rossier BC, Vallet V, Chraibi A, Gaeggeler H-P, and Horisberger J-D (1997). An epithelial serine protease activates the amiloride-sensitive sodium channel. Nature 389, 607–610. [PubMed: 9335501]

Saina M, and Benton R (2013). Visualizing olfactory receptor expression and localization in Drosophila. In Olfactory Receptors: Methods and Protocols, pp. 211–228.

Sato K, Pellegrino M, Nakagawa T, Nakagawa T, Vosshall LB, and Touhara K (2008). Insect olfactory receptors are heteromeric ligand-gated ion channels. Nature 452, 1002–1006. [PubMed: 18408712]

Shi H, Asher C, Chigaev A, Yung Y, Reuveny E, Seger R, and Garty H (2002). Interactions of β and γENaC with Nedd4 can be facilitated by an ERK-mediated phosphorylation. J. Biol. Chem 277, 13539–13547. [PubMed: 11805112]

Siegel RW, and Hall JC (1979). Conditioned responses in courtship behavior of normal and mutant Drosophila. Proc. Natl. Acad. Sci 76, 3430–3434. [PubMed: 16592682]

Smart R, Kiely A, Beale M, Vargas E, Carraher C, Kralicek AV, Christie DL, Chen C, Newcomb RD, and Warr CG (2008). Drosophila odorant receptors are novel seven transmembrane domain proteins that can signal independently of heterotrimeric G proteins. Insect Biochem. Mol. Biol 38, 770–780. [PubMed: 18625400]

Starostina E, Liu T, Vijayan V, Zheng Z, Siwicki KK, and Pikielny CW (2012). A Drosophila DEG/ENaC subunit functions specifically in gustatory neurons required for male courtship behavior. J. Neurosci 32, 4665–4674. [PubMed: 22457513]

Stephan AB, Shum EY, Hirsh S, Cygnar KD, Reisert J, and Zhao H (2009). ANO2 is the cilial calcium-activated chloride channel that may mediate olfactory amplification. Proc. Natl. Acad. Sci 106, 11776–11781. [PubMed: 19561302]

Sun X, Zhao D, Li YL, Sun Y, Lei XH, Zhang JN, Wu MM, Li RY, Zhao ZF, Zhang ZR, et al. (2013). Regulation of ASIC1 by Ca^{2+}/calmodulin-dependent protein kinase II in human glioblastoma multiforme. Oncol. Rep 30, 2852–2858. [PubMed: 24100685]

Thistle R, Cameron P, Ghorayshi A, Dennison L, and Scott K (2012). Contact chemoreceptors mediate male-male repulsion and male-female attraction during Drosophila courtship. Cell 149, 1140–1151. [PubMed: 22632976]

Toda H, Zhao X, and Dickson BJ (2012). The Drosophila female aphrodisiac pheromone activates $ppk23^{+}$ sensory neurons to elicit male courtship behavior. Cell Rep. 1, 599–607. [PubMed: 22813735]

Tokuda S, Niisato N, Morisaki S, and Marunaka Y (2002). Calmodulin-dependent regulation of hypotonicity-induced translocation of ENaC in renal epithelial A6 cells. Biochem. Biophys. Res. Commun 298, 619–623. [PubMed: 12408997]

Vijayan V, Thistle R, Liu T, Starostina E, and Pikielny CW (2014). Drosophila pheromone-sensing neurons expressing the ppk25 ion channel subunit stimulate male courtship and female receptivity. PLoS Genet. 10, e1004238. [PubMed: 24675786]

Vocke K, Dauner K, Hahn A, Ulbrich A, Broecker J, Keller S, Frings S, and Möhrlen F (2013). Calmodulin-dependent activation and inactivation of anoctamin calcium-gated chloride channels. J. Gen. Physiol 142, 381–404. [PubMed: 24081981]

Wang J-W, Beck ES, and McCabe BD (2012). A modular toolset for recombination transgenesis and neurogenetic analysis of Drosophila. PLoS One 7, e42102. [PubMed: 22848718]

Wicher D (2015). Olfactory signaling in insects. Prog. Mol. Biol. Transl. Sci 130, 37–54. [PubMed: 25623336]

Wicher D, Schäfer R, Bauernfeind R, Stensmyr MC, Heller R, Heinemann SH, and Hansson BS (2008). Drosophila odorant receptors are both ligand-gated and cyclic-nucleotide-activated cation channels. Nature 452, 1007–1011. [PubMed: 18408711]

Yao CA, Ignell R, and Carlson JR (2005). Chemosensory coding by neurons in the coeloconic sensilla of the Drosophila antenna. J. Neurosci 25, 8359–8367. [PubMed: 16162917]

Younger MA, Muller M, Tong A, Pym EC, and Davis GW (2013). A presynaptic ENaC channel drives homeostatic plasticity. Neuron 79, 1183–1196. [PubMed: 23973209]

Yu L, Cai H, Yue Q, Alli AA, Wang D, Al-Khalili O, Bao H-F, and Eaton DC (2013). WNK4 inhibition of ENaC is independent of Nedd4–2-mediated ENaC ubiquitination. Am. J. Physiol. Physiol 305, F31–F41.

Zak JD, Grimaud J, Li RC, Lin CC, and Murthy VN (2018). Calcium-activated chloride channels clamp odor-evoked spike activity in olfactory receptor neurons. Sci. Rep 8, 1–13. [PubMed: 29311619]

Zelle KM, Lu B, Pyfrom SC, and Ben-Shahar Y (2013). The genetic architecture of degenerin/epithelial sodium channels in Drosophila. G3 3, 441–450. [PubMed: 23449991]

Zentner MD, Lin HH, Wen X, Kim KJ, and Ann DK (1998). The amiloride-sensitive epithelial sodium channel α-subunit is transcriptionally down-regulated in rat parotid cells by the extracellular signal-regulated protein kinase pathway. J. Biol. Chem 273, 30770–30776. [PubMed: 9804854]

Zhang Y, Tsang TK, Bushong EA, Chu L-A, Chiang A-S, Ellisman MH, Reingruber J, and Su C-Y (2019). Asymmetric ephaptic inhibition between compartmentalized olfactory receptor neurons. Nat. Commun 10, 1560. [PubMed: 30952860]

Zhong L, Hwang RY, and Tracey WD (2010). Pickpocket is a DEG/ENaC protein required for mechanical nociception in Drosophila larvae. Curr. Biol 20, 429–434. [PubMed: 20171104]

Highlights

1. Ionotropic signal amplification occurs in select olfactory receptor neurons (ORNs)
2. Amplification is mediated by Pickpocket 25 (PPK25), a DEG/ENaC member
3. Receptor-mediated influx of Ca^{2+}, serving as a second messenger, activates PPK25
4. A reproductive hormone dynamically regulates PPK25 expression to impact courtship

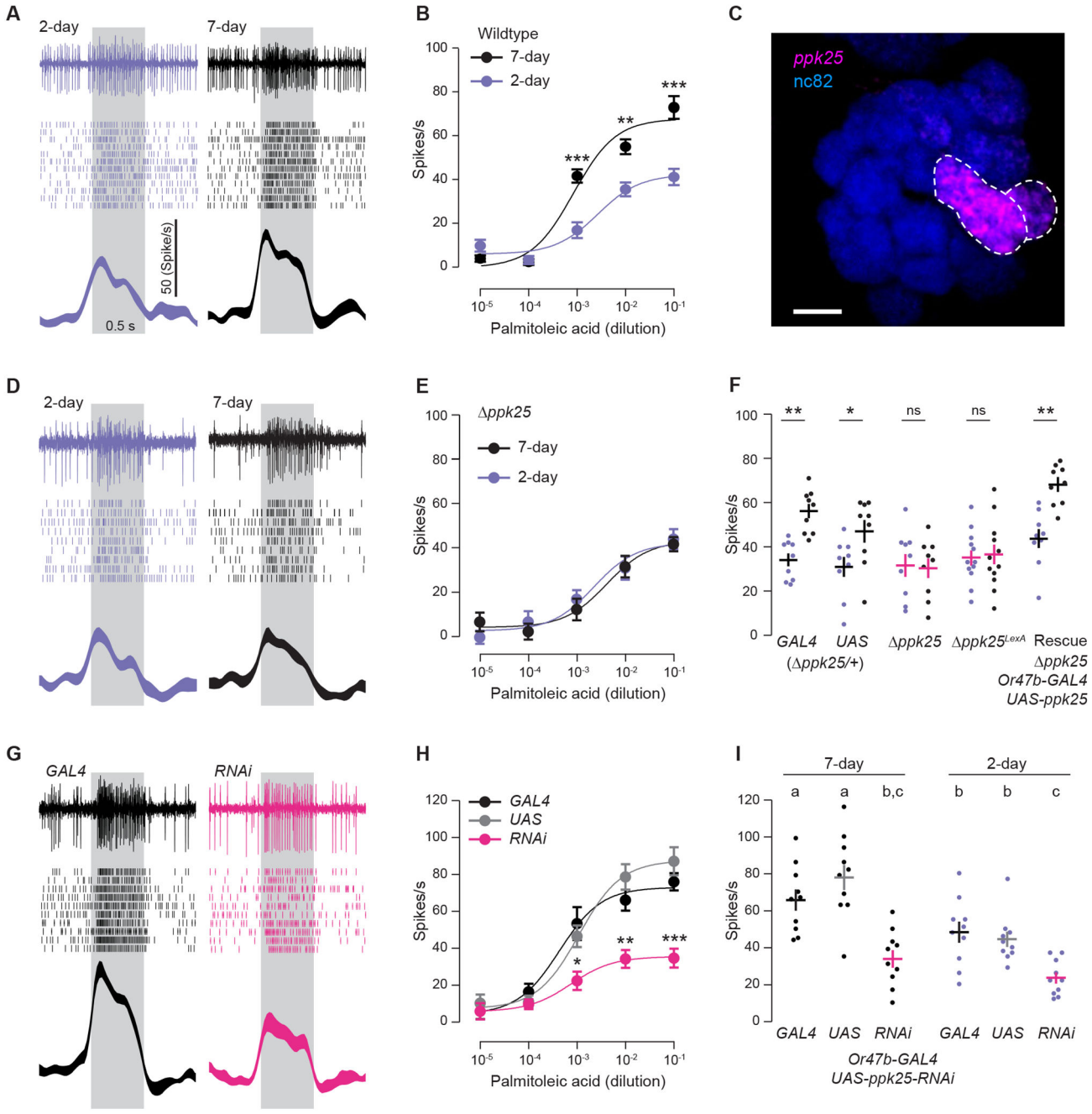

Figure 1. *ppk25* is required for the amplification of Or47b ORN responses.

(A) Single-sensillum recording. Representative traces (top), raster plots (middle), and peri-stimulus time histograms (PSTH, bottom) are shown for Or47b ORN responses in wildtype males (palmitoleic acid, 10^{-2}). Line width: s.e.m. Gray bar: stimulus duration.

(B) Dosage curves of Or47b spike responses from 2d and 7d males. Adjusted peak responses (pre-stimulus baseline activity subtracted from the peak response, see Methods). Parallel experiments, mean ± s.e.m. (n=12, from 6~7 flies). *P<0.05, t-test.

(C) Confocal image of the antennal lobe. *ppk25-GAL4* labeled Or47b and Ir84a ORNs in 7d males (magenta, VAllm and VL2a glomeruli, respectively). nc82: neuropil marker (blue). Scale bar: 10 μm.

(D-E) As in (A-B) except that recordings were performed in *ppk25* mutant males ($ppk25^{\Delta 5\text{-}22}$).

(F) Quantification of Or47b ORN responses to palmitoleic acid (10^{-2}). *Or47b-GAL4* and *UAS-ppk25* heterozygous controls (*Δppk25/+), Δppk25*, another *ppk25* mutant allele ($\Delta ppk25^{LexA}$) and genetic rescue of *ppk25* in the Or47b ORNs. Mean ± s.e.m. (n=9, from 4~6 flies).

(G-H) RNAi knockdown of *ppk25* reduced Or47b ORN responses in 7d males. Sample traces (G) and dosage curves (H) are shown. *P<0.05, **P<0.005, ***P<0.0005, t-test.

(I) Quantification of Or47b ORN responses to palmitoleic acid (10^{-2}). Parallel experiments, mean ± s.e.m. (n=10, from 6~8 flies). ANOVA followed by Tukey's test. Significant differences (P <0.05) are indicated by different letters, for example between the 7d controls (a) and the RNAi group (b, c). No significant differences were observed between groups indicated by the same letters.

See also Figures S1 and S2. Table S1 lists genotypes for all experiments.

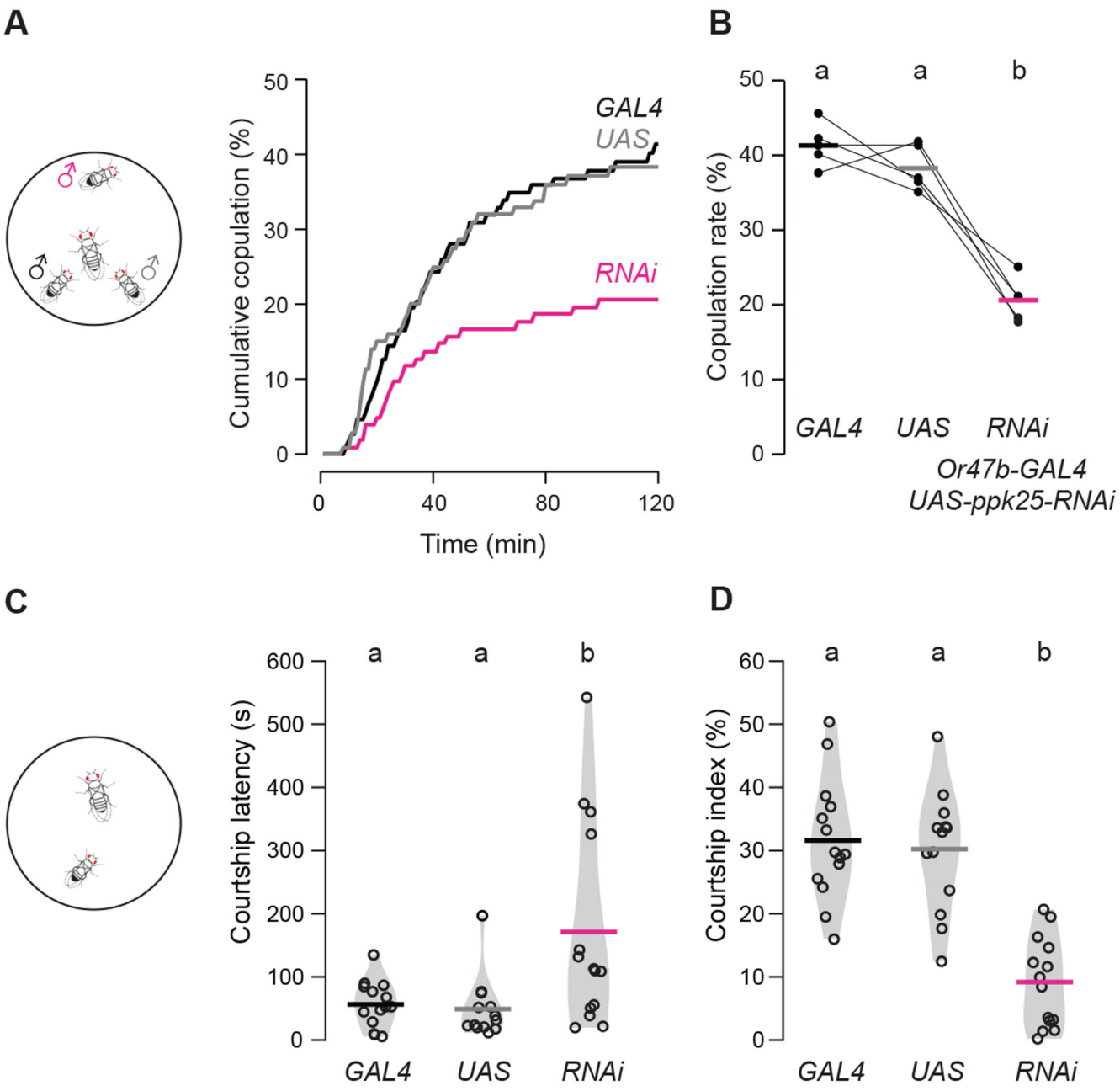

Figure 2. *ppk25* in Or47b ORNs impacts courtship

(A) Courtship competition assays were conducted with one 3d wildtype female and three 7d males of different genotypes: *Or47b-GAL4/+, UAS-ppk25-RNAi/+*, and *Or47b-GAL4/ UAS-ppk25-RNAi*. Cumulative copulation rates over time are shown for each genotype.

(B) Copulation rates at the end of the 2-hr assays. Lines connect results from the same experiments (n=5, total 102 matches).

(C-D) Single-pair courtship assays were conducted with one 3d wildtype female and one 7d male of different genotypes as indicated in (A-B). Courtship latency (C) and courtship index

(D) are shown for each genotype (n=13-14). Horizontal bars: mean. Significant differences (P <0.05) are indicated by different letters, ANOVA followed by Tukey's test.

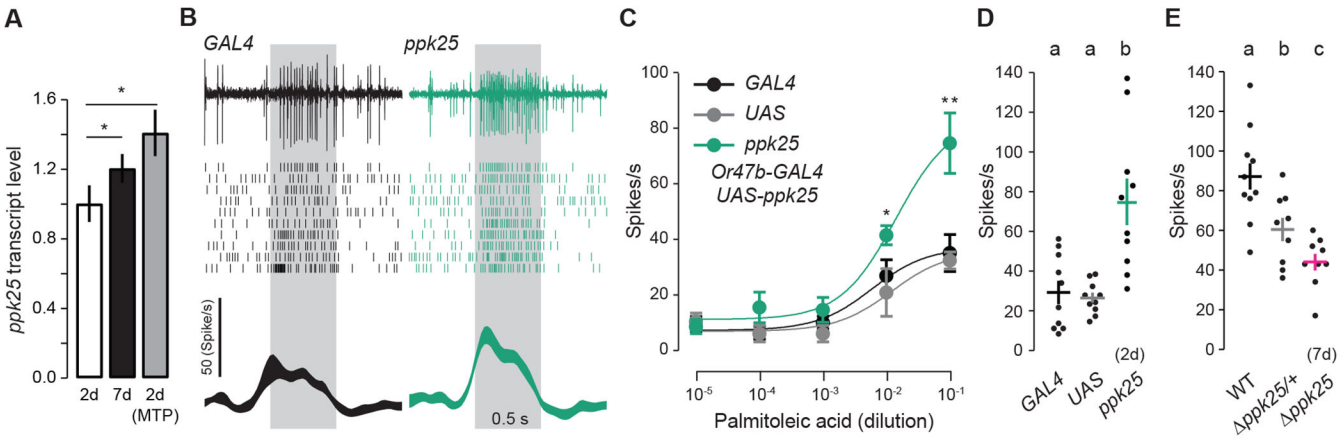

Figure 3. Overexpression of *ppk25* increases Or47b ORN responses in males.

(A) Quantitative RT-PCR of *ppk25* from male antennal mRNA. MTP: methoprene-treated. Expression level is normalized to that of 2d males (n=12; *P<0.05, t-test).

(B-C) Overexpression of *ppk25* elevated Or47b ORN responses in 2d males. Sample traces, raster, PSTH (palmitoleic acid, 10^{-2}) (B) and dosage curves (C) are shown. Adjusted peak responses. *P<0.05, **P<0.005, t-test.

(D) Quantification of Or47b ORN responses to palmitoleic acid (10^{-1}) in 2d males. Parallel experiments, mean ± s.e.m. (n=10, from 6~8 flies).

(E) Comparison of Or47b ORN responses to palmitoleic acid (10^{-1}) in 7d wildtype, *Δppk25/+* heterozygous, and *Δppk25* homozygous mutant males. Mean ± s.e.m. (n= 9~12, from 7~9 flies). Significant differences between any two groups (P <0.05) are indicated by different letters, ANOVA followed by Tukey's test.

See also Figures S3, S4 and S5.

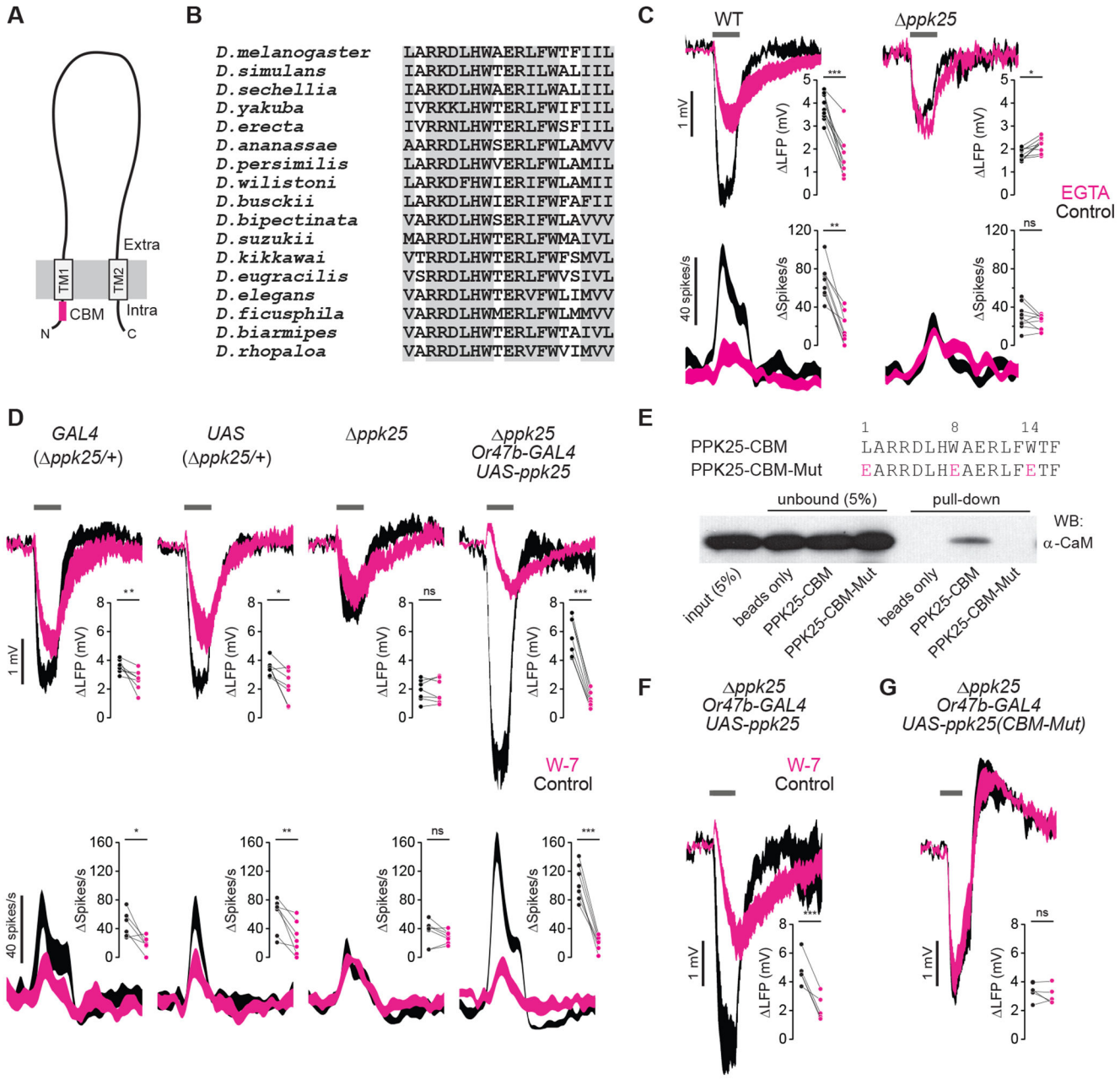

Figure 4. PPK25 is a Ca^{2+}-activated transduction channel in Or47b ORNs.

(A) Topology of PPK25. CBM: calmodulin binding motif.

(B) Multiple sequence alignment. Conserved PPK25 CBM residues are shaded in gray.

(C) Reducing extracellular Ca^{2+} with EGTA attenuated Or47b responses in wildtype (left panels) but not *Δppk25* males (right panels). Top and bottom traces indicate LFP and the corresponding spike responses. Black: control responses; magenta: responses after 5-min application of 5 mM EGTA. Horizontal bar: 0.5-s palmitoleic acid (10^{-2}). Parallel experiments, line width indicates s.e.m. (n=9, from 5~7 flies). Lines connect results from the same neurons.

(D) Similar to (C) except that 500 μm W-7 was used to block CaM (n=7, from 4~6 flies).

(E) CaM binding assay with wildtype or mutant CBM peptides. Numbers are signature hydrophobic residues (top panel). Western blotting with CaM antibody (bottom panel). The input, unbound and pull-down fractions are shown.
(F) Rescuing *ppk25* mutation with wildtype PPK25 and W-7 was used to block CaM (n=5, from 5 flies, right panel).
(G) As in (F) except that PPK25 with 1-8-14 CBM mutations was expressed. *P<0.05, **P<0.005, ***P<0.0005, paired t-test.
See also Figures S6 and S7.

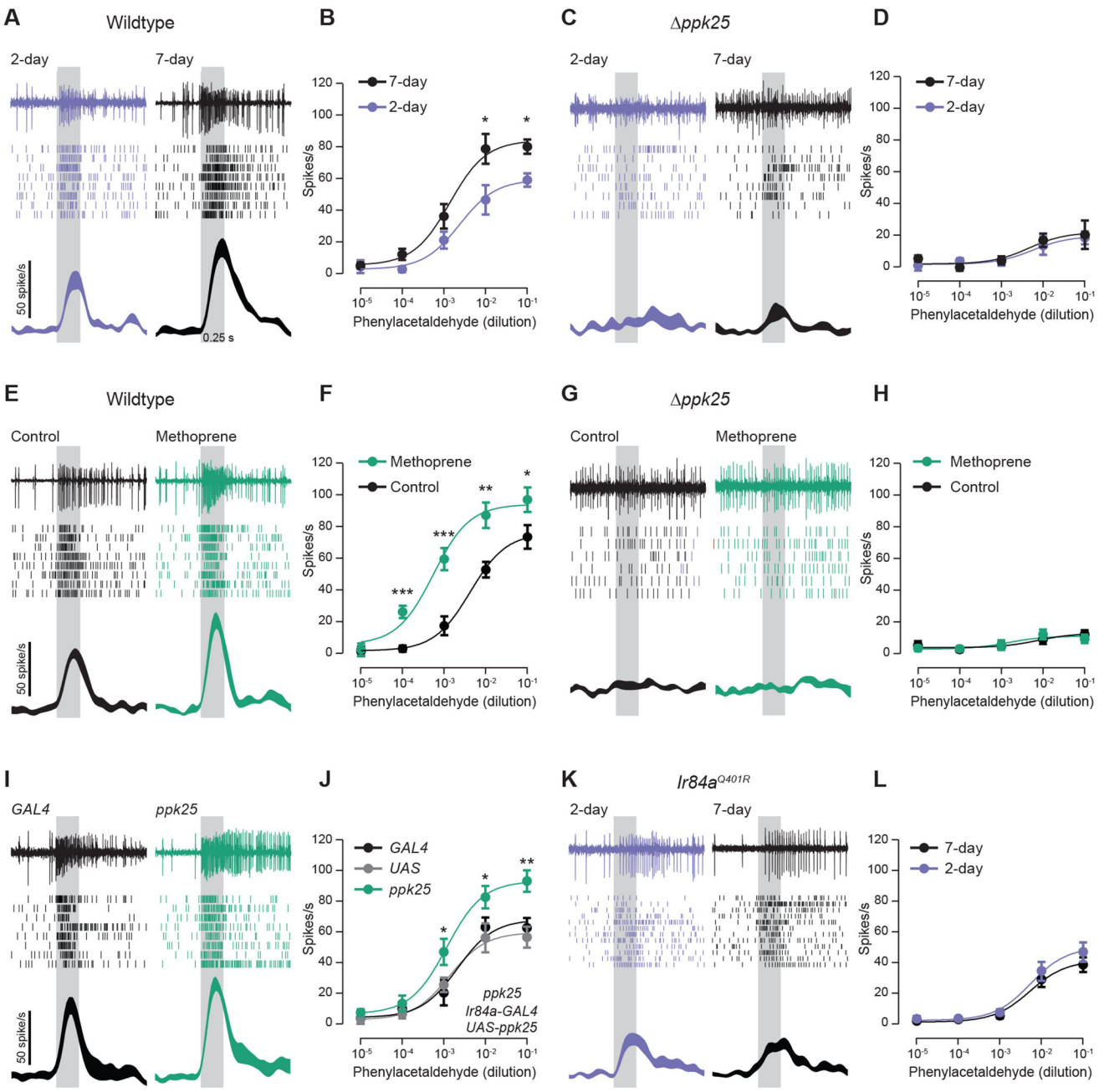

Figure 5. Age-dependent response plasticity in Ir84a ORNs.

(A) Single-sensillum recording. Representative traces (top), raster plots (middle), and PSTH (bottom) are shown for Ir84a ORN responses (phenylacetaldehyde, 10^{-2}). Line width: s.e.m. Gray bar: stimulus duration.

(B) Dosage curves of Ir84a spike responses (adjusted peak responses).

(C-D) As in (A-B) except that recordings were performed in *Δppk25* males (n=8, from 4~6 flies).

(E) Ir84a responses from 2d males treated for two days with solvent (ethanol, control) or methoprene, a synthetic juvenile hormone analog.

(F) Dosage curves of Ir84a spike responses (adjusted peak responses). Parallel experiments, mean ± s.e.m. (n=8, from 4~6 flies).
(G-H) As in (E-F) except that 2d *ppk25* mutant males were examined. Parallel experiments, mean ± s.e.m. (n=6, from 4~6 flies).
(I-J) Overexpression of *ppk25* elevated Ir84a ORN responses in 2d males. Parallel experiments, mean ± s.e.m. (n=8, from 4~6 flies).
(K-L) As in (A-B) except that recordings were performed in $Ir84a^{Q401R}$ males. Parallel experiments, mean ± s.e.m. (n=12, from 8~10 flies). *P<0.05, **P<0.005, ***P<0.0005, t-test.

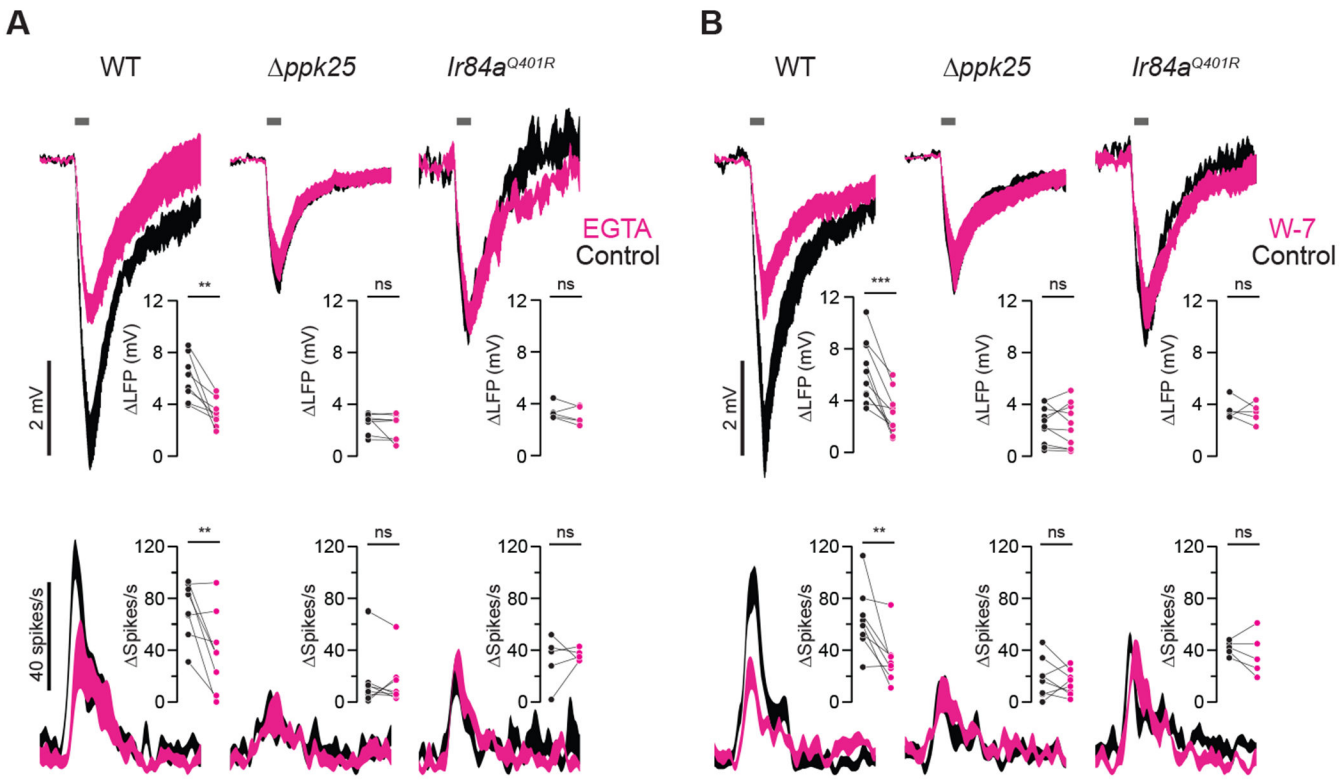

Figure 6. PPK25 also functions as a Ca^{2+}-activated transduction channel in Ir84a ORNs.

(A-B) LFP and the corresponding spike responses from wildtype, *Δppk25*, and *Ir84a*^{Q401R} males (7d). Black: control responses; magenta: responses after 5-min application of 5 mM EGTA (A) or 500 μM W-7

(B). Horizontal bar: 0.25-s phenylacetaldehyde (10^{-2}) (n=5~10, from 4~10 flies). ** P<0.005, *** P<0.0005, paired t-test.

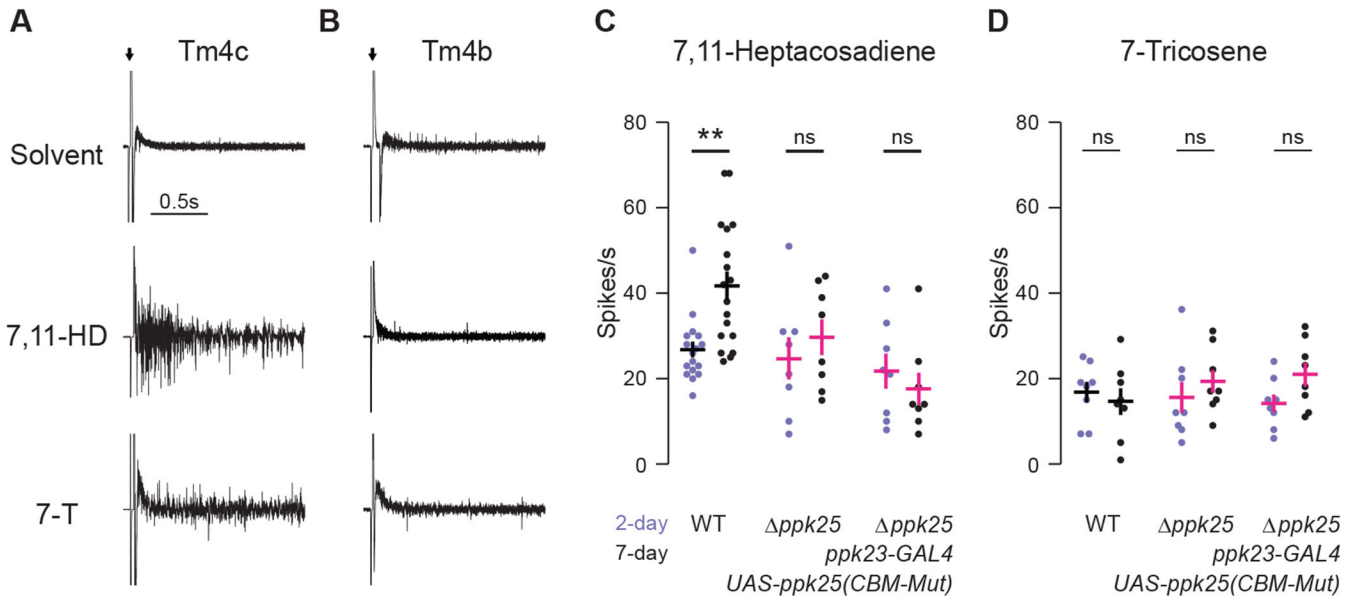

Figure 7. Age-dependent response plasticity in tarsal *ppk25*$^{+}$ GRNs.

(A-B) Tip recording of foreleg gustatory sensilla. Representative traces are shown for Tm4c and Tm4b sensilla in response to solvent (1 mM KCl), 7,11-heptacosadiene (7,11-HD, 20 ng/μl) or 7-tricosene (7-T, 10 ng/μl) from 7d wildtype males.

(C) Quantification of Tm4c GRN spike responses to 7,11-HD from wildtype, *Δppk25*, and *ppk25*-CBM mutant males (n= 8~18, from 6~13 flies). Average spike responses for the first second following tastant presentation are shown. ** P<0.005, t-test.

(D) As in (C) except that the spike responses to 7-T were recorded (n= 8, from 6~8 flies).

Table 1.

Predicted calmodulin binding motifs (CBMs) in the N-terminal intracellular domains of members in the DEG/ENaC superfamily.

DEG/ENaC subunits	Predicted CBMs	Residue numbers
C. elegans		
DEG-1 (CE24854)	AKRVLIARNSFSKL	78-81
DEGT-1 (CE45781)	LHTRYKTWFRVLW	56-68
ASIC-1 (CE45595)	PRAYVSTGWRRYMWLLCF	27-44
DEL-8 (CE43303)	SQALMSKTLRMRIFWWIV	42-59
D. melanogaster		
PPK2 (CG1058)	GIDLTFRRRRKAGSVAC	13-29
PPK6 (CG11209)	MRRNRTYGLSRFI	53-65
PPK7 (CG9499)	IHGLDRLLSAKASR	44-57
PPK15 (CG14239)	QVLRKKRGFGFVTN	10-23
PPK16 (CG34059)	TRQDISRHERWFWLVV	72-87
PPK23 (CG8527)	FLETLVIFRRSLIYQ	16-30
PPK24 (CG15555)	SGRRIQERFFWFV	79-91
PPK25 (CG33349)	LARRDLHWAERLFWTFIIL	29-47
PPK27 (CG10858)	KTSLNGFGLLYFIRKRR	18-34
PPK28 (CG4805)	NTICSRAAIKRSVVYYLKN	28-46
A. aegypti		
PPK06258 (AAEL006258)	TSRKYHYTERLFW	31-43
PPK00926 (AAEL000926) (PPK28-like)	CRERSICEKFWWVVV	34-48
PPK10995 (AAEL010995) (PPK28-like)	HLANRRLTLFE	26-36
PPK14009 (AAEL014009) (PPK23-like)	PFGTVRLLKG SLLYQTK	43-59
M. musculus		
SCNN1G (NP_035456.1)	VSRGRLRRLLW	46-56
ASIC2, isoform MDEG2 (NP_031410.1)	RTAAGGSFQRRALWVL	75-91
ASIC5 (NP_067345.1)	HAEKGLLGKIKRYLS	10-24
H. sapiens		
SCNN1G (AIC49684.1)	VSRGRLRRLLWI	46-57
ASIC5 (NP_059115.1)	VQNRSKIRRVLWLV	54-66

KEY RESOURCES TABLE

REAGENT or RESOURCE	SOURCE	IDENTIFIER
Antibodies		
Myc-Tag (71D10) Rabbit mAB	Cell Signaling Technology	RRID:AB_10693332
Retinal space (21A6) Mouse mAB	Developmental Studies Hybridoma Bank at the University of Iowa	RRID:AB_528449
Goat anti-Rabbit IgG (H+L) Cross-Adsorbed Secondary Antibody, Alexa Fluor 647	Invitrogen	RRID:AB_2535812
F(ab')2-Goat anti-Mouse IgG (H+L) Cross-Adsorbed Secondary Antibody, Alexa Fluor 568	Invitrogen	RRID:AB_143162
Rabbit Anti-Green Fluorescent Protein (GFP) Polyclonal Antibody	Invitrogen	RRID:AB_221569
Rabbit anti-calmodulin antibody	Cell Signaling	RRID:AB_2069270
Bruchpilot (nc82) Mouse mAB	Developmental Studies Hybridoma Bank at the University of Iowa	RRID:AB_2314866
Chemicals (odorants & tastants)		
Ethyl hexanoate	Sigma-Aldrich	CAS:123-66-0
Butyraldehyde	Sigma-Aldrich	CAS:123-72-8
Phenylacetaldehyde	Sigma-Aldrich	CAS:122-78-1
trans-Palmitoleic acid	Cayman Chemical	CAS:10030-73-6
7,11-heptacosadiene	Cayman Chemical	CAS:100462-58-6
7-tricosene	Cayman Chemical	CAS:52078-42-9
Experimental Models: Organisms/Strains		
Drosophila: Or22a-GAL4	Dobritsa et al., 2003	N/A
Drosophila: ppk25$^{A5\text{-}22}$	Lin et al., 2005	N/A
Drosophila: Δppk25^{LexA}	This study	N/A
Drosophila: UAS-ppk25	Vijayan et al., 2014	N/A
Drosophila: ppk25-GAL4	Starostina et al., 2012	N/A
Drosophila: UAS-mcd8-GFP	Bloomington Drosophila Stock Center	RRID:BDSC_5137
Drosophila: UAS-mcd8-GFP	Bloomington Drosophila Stock Center	RRID:BDSC_5130
Drosophila: Or47b-GAL4	Vosshall et al., 2000	RRID:BDSC_9984
Drosophila: UAS-ppk25-RNAi	Perkins et al., 2015	RRID:BDSC_27088
Drosophila: Canton-S	Carlson Lab, Yale University	N/A
Drosophila: Berlin (W^{1})	Lin et al., 2016	N/A
Drosophila: w^{1118}	Lin et al., 2016	N/A
Drosophila: UAS-ppk25-myc	This study	N/A
Drosophila: UAS-ppk25 (1-8-14 mutation)-myc	This study	N/A
Drosophila: Ir84a-GAL4	Silbering et al., 2011	RRID:BDSC_41734
Drosophila: Ir84a^{Q401R}	This study	N/A
Drosophila: ppk23-GAL4	Thistle et al., 2012	N/A
Drosophila: UAS-H134R-ChR2	Pulver et al., 2009	RRID:BDSC_28995

REAGENT or RESOURCE	SOURCE	IDENTIFIER
Drosophila: UAS-Or47b-myc	Hallem et al., 2004	RRID:BDSC_76045
Recombinant DNA		
Plasmid: *pDONR221*	Thermo Fisher Scientific	12536-017
Plasmid: *pBID-UASC-G*	Wang et al., 2012	N/A
Software and Algorithms		
Fiji	NIH	RRID: SCR_002285
Igor Pro 6.32A	WaveMetrics	RRID: SCR_000325
Clampfit 10.7	Molecular Devices	https://www.moleculardevices.com
MATLAB	MathWorks	RRID: SCR_001622